Volume 6 APRIL, 1935 Number 4

PHYSICS

A Journal of General and Applied Physics

The Telegraphist's Equations at Ultra-High Frequencies

RONOLD KING, *Department of Physics, Lafayette College, Easton, Pennsylvania*

(Received November 1, 1934)

The telegraphist's or long line equations are derived from the Maxwell field equations for ultra-high frequencies. By taking into account retardation and the time rate of change of current, a new circuit parameter is obtained in addition to the four usually found in the conventional low frequency equations. This new parameter integrates into the radiation resistance of the parallel wires. The approximations involved are discussed, and application is made to a specific example.

IT is being increasingly realized that ultra-high frequencies (electromagnetic oscillations of wavelengths from a few centimeters to about five meters), are more than a scientific curiosity. The production of these microwaves and their properties have been intensively studied in recent years, and they have been successfully used in the field of very short wave radio communication.[1] In physical and physical-chemical investigations dealing with the structure of matter, such as, for example, the measurement of dielectric constants, and the determination of molecular size, the use of ultra-high frequencies may prove extremely productive.[2]

However, experimental technique and electric circuit theory differ very significantly at ultra-high frequencies from the corresponding low frequency problems. Entirely new methods must be devised and justified theoretically, if accurate measurements of capacitance or conductance, for example, are to be made. The analytical treatment of circuits with lumped constants has been outlined by Brainard.[3] He has shown that a better approximation in handling such circuits is obtained by writing the impedance operator in the form, $(R+j\omega L+\omega^2 N)$, instead of in the conventional low frequency form, $(R+j\omega L)$. The added term represents the radiation resistance. N is a constant which Brainard has called the radiactance of the given circuit element. Actually it becomes increasingly meaningless to speak of lumped constants at all, as the wavelength in question becomes comparable with the linear dimensions of the circuit element. In such cases parallel wire methods are advantageously used for tuning and measuring purposes.[4] Low frequency parallel wire theory depends upon the solution of the telegraphist's equations which, for a sinusoidal current variation, may be written in the following form. I_1 and V_1 are, respectively, current and voltage amplitude.

$$\begin{aligned}(j\omega l+r)I_1&=-dV_1/dx,\\(j\omega c+g)V_1&=-dI_1/dx.\end{aligned}\qquad(1)$$

Here r, l, c and g are, respectively, resistance, inductance, capacitance and leakage conductance per loop unit length of the parallel wires.

[1] An excellent summary of the production, properties and applications of microwaves is given by H. E. Hollmann, Hochfrequenztechnik u. Elektroakustik **44**, 37 (1934).

[2] J. G. Chaffee, Proc. I. R. E. **20**, 1009 (1934), has discussed the use of conventional low frequency methods for measuring dielectric constants up to frequencies of 20 megacycles (wavelengths down to 15 meters).

[3] Brainard, Proc. I. R. E. **22**, 395 (1934).

[4] The problem of electrical measurements at ultra-high frequencies is analyzed by the writer in another paper. R. King, Proc. I. R. E. **23** (1935).

These equations are usually derived in a way presupposing a knowledge of the fact that r, l, c and g are the only circuit parameters which enter into the long line problem.[5] Formulas for these parameters are then derived separately,[6] but always under the assumption that the current amplitude is the same at all points along the wires. This method of analysis is usually adequate at low frequencies when circuit dimensions are small compared with the wavelength. At very high frequencies, on the other hand, the mathematical problem becomes extremely complicated, and it is doubtful whether an exact solution in terms of current, voltage, and a set of circuit parameters is at all possible in any general sense. The following analysis does not pretend to provide such a solution. On the other hand, just as Brainard[3] generalized the impedance operator by introducing a term to account for radiation and thus approximated high frequency conditions in lumped circuits more closely than with the conventional operator, so it is possible to derive a pair of generalized telegraphist's equations which, since they include a radiation term, are a better approximation to the high frequency long line problem than Eqs. (1).

A generalized form of (1) may be derived directly from the Maxwell field equations.[7] Beginning with the equation (rational units) :[8]

$$\text{curl } E_1 = -j\omega B_1/c, \tag{2}$$

one obtains at once, upon applying Stokes' theorem, the expression :

$$\int (E_1, ds) = -j(\omega/c)\int B_{1,\,n} d\sigma. \tag{3}$$

Here $d\sigma$ is an element of the surface bounded by a curve of which ds is an element.

In the case of the parallel wires one chooses for the surface of integration a rectangle bounded by opposite elements dx of the two wires. Then the integral on the left can be shown to be :

$$\int (E_1, ds = dV_1 + cI_{1,\,x} r(\omega) dx. \tag{4}$$

Here $dV_1 = V_{1,\,x} - V_{1,\,x+dx}$, with $V_{1,\,x}$ the amplitude of the voltage difference between the wires at the point x ; $I_{1,\,x}$ is the amplitude of the total current traversing a cross section of the conductor at the point x ; $r(\omega)$ is the resistance per loop unit length of the parallel wires at the frequency $\omega/2\pi$. The step from (3) to (4) depends upon a restrictive assumption that the current density vector, *viz.*, i, is approximately equal to i_x, where i_x is the component along the wires. That is, it is assumed that the current along the conductors is very much greater than the leakage current through the dielectric between them, per unit length.[9]

In order to evaluate the integral on the right of (3), the expression for B as a function of I_x must be known. By considering each element dx of the conductor to be an oscillating dipole of moment p, and integrating over the length of the conductor, one may use the formula,[10]

$$B = \{[\ddot{p}, r]\}/4\pi c^2 r + \{[\dot{p}, r]\}/4\pi c r^2, \tag{5}$$

by setting, $\dot{p} = cI_{1,\,x} e^{j\omega t}$. This gives the expression :

$$B_1 = (I_{1,\,x}/4\pi)\int (1/r^2)(1 + j(\omega/c)r) \times e^{-j(\omega/c)r} \sin(x, r) dx. \tag{6}$$

Important considerations in the steps between (5) and (6) include taking note of the fact that the retarded time $\tau = t - r/c$, and setting $B = B_1 e^{j\omega t}$. It is also to be noted that in taking $I_{1,\,x}$ out from under the sign of integration, one assumes that it is independent of the variable x, and hence, that the current amplitude is uniform over the entire length of the conductor. Hence, (6) gives the flux density amplitude at a point P due to a uniform current in a straight conductor. By defining the distance from P to the

[5] A. Hund, Scientific Paper of the Bureau of Standards, No. 491, p. 520.

[6] Bennett and Crothers, *Electrodynamics for Engineers*, pp. 193, 534; (McGraw-Hill).

[7] The derivation of the long line Eqs. (1) from the field equations was first suggested to the writer by Professor Edward Bennett of the University of Wisconsin.

[8] Mason and Weaver, *The Electromagnetic Field*, p. 264 (Chicago Univ. Press).

[9] For details, see Appendix I.

[10] Mason and Weaver, *The Electromagnetic Field*, p. 311, (Chicago Univ. Press).

conductor to be y, and transforming the integrand, one obtains:

$$B_1=(I_{1,\,x}/4\pi)\int(y/r^3)[(\cos(\omega r/c)+(\omega r/c)\sin(\omega r/c))-j(\sin(\omega r/c)-(\omega r/c)\cos(\omega r/c))]dx. \quad (7)$$

To carry out the integration, the trigonometric functions are expanded in series and integrated term by term. This integration yields:

$$B_1\doteq(I_{1,\,x}/4\pi)[((2/y)-(y\omega^2/c^2)\log(X/y)-X^2y\omega^4/32c^4)-j(Xy\omega^3/3c^3-X^3y\omega^5/360c^5)]. \quad (8)$$

Here X is the length of one conductor. The fact that only a few terms of the series are retained in (8) implies certain restrictions on the relative magnitudes of y, ω and X, as well as the assumption that the point P is not near the end of the conductor. The restrictions will be considered below.

If the diameter of each wire is d, and their separation is a, the total flux due to the currents in both wires (assumed equal and opposite) through the area of length dx between the wires is:

$$\Phi=2\int_{d/2}^{a}B_{1,\,n}dy. \quad (9)$$

Using the value of B_1 obtained in (8), this becomes:

$$\Phi=(I_{1,\,x}/\pi)(\log(2a/d)-j(a^2X\omega^3/12c^3)), \quad (10)$$

if only the leading real and imaginary terms are retained. In neglecting higher powered terms it is assumed that the following conditions are satisfied:

$$d^2\ll a^2\ll X^2,\quad X^2\omega^2/120c^2\ll 1,$$
$$(a^2\omega^2/4c^2)(\log(X/a)+X^2\omega^2/32c^2+\tfrac{1}{2})\ll\log(2a/d). \quad (11)$$

It is also assumed, and this is true at high frequencies, that the current flows in a thin layer on the surface of the conductors. The conditions (11) are examined for a specific case in Appendix II.

With (10) the right side of (3) becomes:

$$-j(\omega/c)\int B_{1,\,n}d\sigma=-j(\omega/c)\Phi=-(I_{1,\,x}/c)(j\omega l+\omega^4nX). \quad (12)$$

$$\text{Here, } l=(1/\pi)\log 2a/d=\text{inductance per loop unit length;}\quad n=a^2/12c^3=\text{radiactance per loop unit length.} \quad (13)$$

By combining (12) with (4) according to (3), one has:

$$dV/dx=-(I/c)(rc^2+j\omega l+\omega^4nX). \quad (14)$$

In this equation all quantities are measured in rational units; subscripts have been omitted with the understanding that only amplitudes and not instantaneous values of current and voltage are involved.

The second generalized equation is derived from:

$$\operatorname{div} i+\partial\rho/\partial t=0, \quad (15)$$

$$\operatorname{div}\epsilon E=\rho. \quad (16)$$

Since $a^2\gg d^2$, one may assume cylindrical symmetry to prevail about each conductor, and write (15) in cylindrical coordinates independent of the angle. By integrating over the cross-sectional area of the conductor, one obtains:

$$\partial I_x/\partial x=-I_y-\partial q/\partial t. \quad (17)$$

Here $I_x=\int i_x d\sigma$, and $q=\int\rho d\sigma$. I_y is the total current leaving or entering unit length of the conductor in a radial direction.

By a generalized Ohm's law, one now writes:

$$I_y=gV. \quad (18)$$

Here V is the potential difference between the wires at dx, and g is the radial volume conductivity (leakage conductance or leakance) per unit length of the medium between the wires. It may be a function of frequency. An expression for g is easily obtained by analogy with an electrostatic problem. In rational units it is:

$$g=2\pi\sigma_m/c\log(2a/d). \quad (19)$$

Here σ_m is the volume conductivity of the medium at a frequency $\omega/2\pi$.

By now applying the divergence theorem to (16) and integrating, it is not difficult to show that,[11]

$$q=CV \quad (20)$$

[11] See Appendix III.

where, $C=\pi\epsilon/\log(2a/d)=$ capacitance per loop unit length. (21)

Upon substituting (20) in (17) one at once obtains the second long line equation. It is, in rational units:

$$dI/dx=-V(g+j\omega C). \tag{22}$$

Upon changing to practical units one has, from (14) and (22), the following pair of equations corresponding to (1):

$$\begin{aligned} dV/dx&=-I(r+r_r+j\omega l),\\ dI/dx&=-V(g+j\omega C). \end{aligned} \tag{23}$$

The circuit parameters are defined by:

r (ohms) obtained from skin effect formulas;[12]
l (henries) $=4\log(2a/d)\times10^{-9}$;
C (farads) $=\epsilon/4\log(2a/d)\times10^{9}$;
g (mhos) $=2\pi\sigma_m/\log(2a/d)$;
r_r (ohms) $=10a^2X\omega^4/c^4$.

These parameters are all defined per loop unit length of the parallel wires.

It is clear that by writing $r'=r+r_r$, (23) reduces formally to (1). It is easily shown that corresponding to a total resistance rX for a pair of wires of length X, one has a quantity,

$$R_r=Xr_r=40\pi^2(X/\lambda)^2(2\pi a/\lambda)^2. \tag{24}$$

This quantity R_r is the radiation resistance of a pair of wires of length X, separation a, at a wavelength λ. Precisely the same formula may be derived using Poynting's theorem, provided one assumes a uniform current distribution, as was done in deriving (23). Evidently, then, Eqs. (23) include as an additional circuit parameter the energy radiated from the parallel wires. It is clear that at low frequencies r_r becomes vanishingly small compared with r, whereas it becomes comparable in magnitude to r at frequencies corresponding to $\omega=10^9$.

In deriving the expressions for the circuit parameters, the assumption was made throughout that the current amplitude is independent of x. If this is not done the mathematical problem becomes extremely complicated, and a representation in terms of simple circuit parameters is no longer possible. It is, however, possible to correct the parameters individually for non-uniform current distribution. This procedure is well known in obtaining the radiation resistance of antennas. It goes without saying that the entire method of carrying out a first integration of the field equations in order to obtain equations involving current and voltage rather than the field vectors B and E is not very satisfactory in any case. Certainly the differential equations obtained and the circuit parameters which are involved are rather crude approximations. Nevertheless, (23) is a better approximation to the ultra-high frequency case than (1). In fact, it shows the limitations implied in the customary method of adding ohmic and radiation resistance to obtain the total or effective resistance.

From the present discussion it is evident that the mathematical problems encountered in handling ultra-high frequency circuits are certainly no less complicated than the experimental ones. Since, however, it can hardly be a question of making measurements at ultra-high frequencies with the precision common in low frequency work, it may be concluded that a satisfactory qualitative understanding, and in some cases quantitative approximations to experimental conditions may be secured by means of the mathematical theory here developed. An illustration of such an application is, for example, the measurement of the resistance of coils and short lengths of wires at an ultra-high frequency.[4] From a solution of (23) with boundary conditions appropriate for a parallel wire system with general terminal impedances, a formula is derived for use in experimentally measuring the effective lumped resistance of a coil or wire. The resistance so measured includes the high frequency ohmic resistance R, and the radiation resistance ω^2N, as explained by Brainard.[3] For simple cases these two terms can be separated.

Without going into further detail, it should be clear of what fundamental significance in all work dealing with ultra-high frequencies is a clear understanding of the difficulties involved, and of the limitations of both theory and experiment. A mere extrapolation of low frequency methods and theory is not adequate.

Acknowledgment

The writer is indebted to Dr. G. H. Brown, formerly at the University of Wisconsin, for reading the manuscript and making valuable suggestions.

[12] A. Hund, *High Frequency Measurements*, p. 265; (McGraw-Hill).

Appendix I

In carrying out the integration on the left side of (3) it must be recalled that,

$$E_1 = -\nabla V_1 - j(\omega/c)A_1,$$

where A is the vector potential defined by, $B = \text{curl } A$. Hence, in order to make it possible to write,

$$E_y = -\nabla_y V = -\partial V/\partial y,$$

it is necessary that $A_y \doteq 0$, or, what is the same thing, $A \doteq A_x$. (The variable y stands for the radial distance from the conductor.) In view of the relation,

$$(\nabla^2 + \omega^2/c^2)A_1 = -i_1/c,$$

it follows that, $i \doteq i_x$ must be true.

Appendix II

In carrying out the measurements described in reference 4, the following constants were used: $\omega = 10^9$; $a = 5$ cm; $d = 0.08$ cm; $X \doteq 10^2$ cm. The circuit parameters were computed to be:

$r = 2.65 \times 10^{-2}$ ohm/loop cm;
$l = 1.93 \times 10^{-8}$ henry/loop cm;
$C = 5.76 \times 10^{-14}$ farad/loop cm;
$g = 10^{-16}$ mho/loop cm;
$n = 3.1 \times 10^{-40}$ pract. unit/loop cm;
$r_r \doteq 3 \times 10^{-2}$ ohm/loop cm.

With these values, restrictions (11) become:

$$(d^2 = 0.0064) \ll (a^2 = 25) \ll (X^2 = 10^4);$$

$$(X^2\omega^2/120c^2 = 0.109) \ll 1;$$

$$((a^2\omega^2/4c^2)[\log (X/a) + X^2\omega^2/32c^2 + \tfrac{1}{2}] = 0.048) \ll (\log (2a/d) = 4.82).$$

It is clear that these conditions are well satisfied for this case. It is to be noted that r_r is of the same order of magnitude as r.

Appendix III

The integration is:

$$q = \int \epsilon E_n d\sigma = \epsilon(2\pi y E_y dx + \pi y^2 dE_x).$$

The surface of integration is a cylindrical element of the conductor of length dx and radius y. Then applying Ohm's law in the conductor,

$$q = (2\pi\epsilon y E_y - (c\epsilon/\sigma) dI_x'/dx).$$

Here I_x' is the total current in a cross section of radius y. In order to set $dI_x'/dx = 0$, and obtain $E_y = q/2\pi y\epsilon$, it follows that the current must be assumed independent of x, and hence a constant with respect to x. To set $E_y = -\partial V/\partial y$, to permit integration, involves the same assumptions discussed in Appendix I.

APRIL, 1935 PHYSICS VOLUME 6

The Mechanism of the High Velocity of Propagation of Lightning Discharges

A. M. Cravath and L. B. Loeb, *University of California*

(Received January 29, 1935)

Observations by Schonland and Collens with Boys' camera show that the luminous tip of the leader stroke of the lightning discharge advances with a high velocity sometimes exceeding 3×10^9 cm per second. From the fact that electrons traveling 10^9 cm per second produce about 6000 new electrons per cm of actual path and that 6000 new electrons per cm in the direction of the field (i.e., $\alpha = 6000$) requires 4×10^6 volts per cm shows that to give the electrons a velocity in the direction of the field of 10^9 cm per second would require a field exceeding 4×10^6 volts per cm even at the tip of the stroke. The fields, and therefore the electron velocities, are certainly far less than this value. Accordingly the velocity of the tip greatly exceeds the velocity of the electrons in the tip. It is possible to account for this velocity as follows: Calculations based on justified assumptions concerning the conditions known to exist in a lightning stroke show that if the field just ahead of the tip averages 10^5 volts per cm for about one centimeter, ionization by collision by the electrons present in the gas before the stroke would be great enough to advance the tip at the observed rate. Such a field is found not too high to be consistent with the low conductivity of the leader path. In this way a propagation of the leader stroke of a velocity many times higher than the velocity of the electrons can be attained.

THE beautiful observations of Schonland and Collens[1] with the Boys camera have shown that the typical lightning stroke to ground starts with a "leader stroke" whose luminous tip travels with high velocity in the direction from cloud toward ground. The average of measurements of this velocity was greater than 8×10^8 cm/sec. and the maximum exceeded 3×10^9 cm/sec. Schonland and Collens suggested that the electrons in the tip of the "leader" were moving with these velocities, and they correlated the intensities of the leader strokes with the

[1] Schonland and Collens, Proc. Roy. Soc. **A143**, 654 (1934).

values of Townsend's α, the number of ion pairs formed per electron per cm of path in the direction of the field, at the corresponding velocities.

On further consideration it seems certain, however, that the electrons cannot be traveling with these velocities. The fields necessary to produce such velocities have not been measured but we can find a lower limit.

An electron with an actual speed along its path of $U=10^9$ cm/sec. produces by collision 6000 electrons per cm of path.[2] If the velocity W in the direction of the field is 10^9, U is greater than 10^9, and the ionization per cm path is less than 6000, but the path length exceeds the distance traveled in the direction of the field by a larger factor. α is therefore greater than 6000. From Townsend's data[3] we find that $\alpha=6000$ requires a field $X=4\times10^6$ volts/cm. Hence 4×10^6 volts/cm is a lower limit to the field required to produce a velocity $W=10^9$ cm/sec. which is only a third of the highest velocity observed.

The writers wish to point out a mechanism of propagation involving only electron velocities far less than the propagation velocity which they believe comes into play at lower field strengths and thus prevents the field from ever reaching the value necessary to give electrons the propagation velocity.

In the intense field just ahead of the advancing tip of the stroke, the initial free electrons due to ordinary atmospheric ionization multiply rapidly by ionization by collision. Our theory is that they propagate the stroke. The electrons in the stroke channel are the offspring of the initial electrons which were present before the arrival of the stroke. It is not necessary for the stroke to furnish the parent electrons, and therefore not necessary for any electrons to move with the velocity of advance of the stroke. The following crude calculations are sufficient to show how this process can actually take place to the extent and in the manner necessary to propagate the stroke.

Let us arbitrarily assume, to begin with, that the stroke has already developed to a length of 0.2 km, that the channel has a radius of 1 cm at the tip and 10 cm at a distance from the tip, that the tip is advancing 10^9 cm/sec., and that the stroke channel is a good enough conductor to create a tip potential of 10^6 volts relative to the space at a large distance to one side of the tip. This potential is less than 0.01 of that which would be produced by a perfect conductor if the field preceding the stroke in the region of the first 0.2 km exceeded 10 kv/cm, and is therefore not incompatible with the weakness of ionization of the leader channel.

The charge per unit length and the field of such a conductor have been very roughly determined by a cut and try process of adding uniform linear charge distributions of various lengths, for which the field is well known,[4] to the charge distribution of a conducting ellipsoid in a field parallel to its axis, which charge together with its field is also well known.[4] The charges were chosen so as to produce an equipotential of shape differing not too greatly from the channel assumed above. The charge per unit length is of the order of 2×10^{-7} coulomb per cm. The average field over a distance of 1 cm in advance of the tip is about 100 kv/cm. The current in the channel can be calculated from the charge distribution and the propagation velocity by means of the equation of conservation of charge. It is of the order 200 amp. The electron velocity W at the tip where the field is $\sim$100 kv/cm is $\sim3\times10^7$ according to Townsend. The number of electrons required for a current of 200 amp. is therefore $n\sim200/(3\times10^7\times1.6\times10^{-19})\sim4\times10^{13}$ electrons per cm. Since it takes the tip 10^{-9} sec. to advance 1 cm, there is a field of $\sim10^5$ volts/cm acting for $\sim10^{-9}$ sec. in advance of the tip. The electron density will increase by ionization by collision in this interval by the factor $e^{\alpha x}=e^{\alpha Wt}=e^{1000\times3\times10^7\times10^{-9}}=e^{30}=10^{15}$. Hence if there were 6 initial electrons per cm along the axis of the stroke within a distance of the order of 1 cm from the axis, i.e., something less than 6 initial electrons per cm^3, the above mechanism with the potential and radius assumed would produce the necessary number of electrons (4×10^{13} per cm) to propagate the stroke with the assumed velocity. We may now discuss the numerical as-

[2] Brode, Rev. Mod. Phys. **5**, 270 (1933).
[3] Townsend, *Electricity in Gases*, p. 282.
[4] e. g., Ollendorf, *Potentialfelder der Elektrotechnik*.

sumptions that we have used. First, the variation of length of stroke path during most of the growth, i.e., from 0.1 km to several km, has but little effect on the field and charge distribution; the potential difference between the tip and the space at a distance to one side being the important quantity. The radius is not given by observation but we can verify that our estimate is right in order of magnitude. Suppose, for instance, that we had assumed a tip radius of 1 mm instead of 1 cm. Since α is limited, increasing but slowly above 100 kv/cm, we would have found that the ionization by collision could not be confined to the small region just in front of the 1 mm tip, but that a sufficient tip field to produce the necessary ionization in front of the tip would reach out far enough in all directions to produce comparable ionization at more than 1 mm from the axis, thus causing the radius to swell. On the other hand, if we had chosen 10 cm as the radius, the ten-fold increase in the distance at which the field still has a given fraction of its maximum would have resulted in a large reduction of the maximum field necessary. At this lower field, α varies rapidly with field. Since the multiplication factor for ionization by collision is very sensitive to small changes in α, the high ion density would be confined to the neighborhood of the axis where the field had its maximum, and the radius would thus shrink. The above applies only to the radius of the tip. At a long distance from the tip, the radial field at the surface of the channel cannot exceed $\sim$25 kv/cm; ionization by collision will cause the radius to grow continually until the field no longer exceeds this value. The resulting final radius far from the tip would be $\sim$10 cm for the assumed tip potential of 10^6 volts. The assumed velocity of propagation, 10^9 cm/sec., lies well within the range of velocities observed. If we had assumed a smaller velocity we would of course have required less rapid ionization, and hence lower tip field and potential. Roughly, $\int \alpha W dt$ must remain equal to $\sim$30 when the velocity and field vary. A change of initial electron density from $6/cm^3$ to $1/cm^3$ or $1000/cm^3$ would have entirely negligible effect.

In our ignorance of the more precise values of the factors involved any greater accuracy is out the question. It appears, however, that with the assumptions made it is possible to explain the high velocities of propagation of the leader strokes observed in a satisfactory manner without invoking any excessively high electron velocities. It is probable that the above mechanism could be qualitatively applied to explain many of the other phenomena observed by Schonland and others, such as the main stroke, branching and the repeated strokes as well as intermittence. However, such discussion had best be postponed until more data are available.

APRIL, 1935 PHYSICS VOLUME 6

The Coercive Force of Magnetite Powders[1]

V. H. GOTTSCHALK, *Metallurgical Division, U. S. Bureau of Mines*

(Received December 20, 1934)

The coercive force of magnetite powder is increased by mere mechanical grinding. Measurements on sized powders of one natural and one artificial magnetite give a linear relation between coercive force and mean specific surface of the grains. It is suggested that this relation between coercive force and specific surface may prove to be important in deciding between theories of ferromagnetism.

THE data submitted in this paper are selected from a series of magnetic measurements on sized powders of a number of purified magnetites.[2] Coercive force only is considered at this time, because coercive force varies little if at all with the shape and form of the substance tested but

[1] Published by permission of the Director, U. S. Bureau of Mines. (Not subject to copyright.)

[2] To be described in detail in a forthcoming report of investigations, Metallurgical Division, U. S. Bureau of Mines.

TABLE I. *Hysteresis data for Hayden slag magnetite powders, showing effect of grinding.* (Density of magnetization, $4\pi I$, in gauss.)

FIELD STRENGTH, H, (oersteds)	1 ORIGINAL POWDER −150+200 mesh	2 (1) GROUND TO −325 mesh	3 ORIGINAL POWDER −270+350 mesh	4 (3) GROUND TO −325 mesh	5 (4) GROUND FINER
2700	2640	2539	2876	3244	2822
1745	2440	2400	2763	3122	2669
1250	2395	2220	2608	2968	2500
875	2130	2000	2358	2720	2270
489	1683	1589	1847	2215	1863
245	1080	1130	1254	1614	1430
134	725	850	853	1199	1141
77	479	645	592	916	946
48	321	530	442	747	836
34	247	473	367	664	784
19	144	401	270	552	711
4	50	331	173	438	640
−10	−35	248	66.5	311	565
−41	−236	47	−177.2	0.8	376.7
−97	−490	−355	−545	−539.1	−26.6
−205	−945	−738	−1041	−1231	−700
−450	−1600	−1450	−1739	−2051	−1548
−835	−2254	−1945	−2310	−2656	−2154
−1210	−2400	−2183	−2583	−2936	−2449
−1700	−2520	−2372	−2752	−3109	−2649
−2700	−2640	−2539	−2876	−3244	−2822
PERCENT Fe_3O_4	91.3	91.3	94.9	94.9	94.9
PACKING DENSITY (g $Fe_3O_4 \cdot cm^{-3}$)	2.43	2.40	2.70	3.06	2.76
H_c (oersted (by numerical interpolation))	4.2	49.4	18.4	41.0	93.3
B_r (gauss (by numerical interpolation))	25.7	307.0	142.5	402.0	619

TABLE II. *Hysteresis data for artificial lodestone (reduced hematite) showing effect of grinding.* (Density of magnetization, $4\pi I$, in gauss.)

Analysis, percent:

Fe_3O_4	60.04 (calculated from FeO)
Fe_2O_3	29.53
MnO	None
TiO_2	None
MgO	0.58
SiO_2	7.92
Undet.	1.93

FIELD STRENGTH, H, (oersteds)	1 −80+250 mesh	2 (1) GROUND TO −325 mesh	3 (2) GROUND FINER
3339	1506	1612	1515
2070	1400	1497	1408
1450	1281	1379	1301
925	1152	1240	1176
502	962	1035	990
241	787	849	817
136	683	739	719
79	618	674	660
50	584	640	632
37	569	624	617
20	548	603	601
7	531	584	585
−6	512	564	570
−38	+467	+517	+531
−75	+366	+421	+443
−181	+92.3	+164.6	+221.5
−450	−566.7	−539.1	−443.9
−880	−1027	−1090	−1012
−1360	−1233	−1326	−1246
−2010	−1375	−1480	−1392
−3339	−1506	−1612	−1515
PACKING DENSITY (g $Fe_3O_4 \cdot cm^{-3}$)	1.527	1.622	1.594
H_c (oersted (by numerical interpolation))	220	245	271
B_r (gauss (by numerical interpolation))	522	573	577

is characteristic of the material itself.[3] The data for remanence, for example, were found to require large corrections for shearing and for concentration or packing density; both of these corrections appear to have minor influence on coercive force.

EXPERIMENTAL RESULTS

The magnetic measurements were made by a modified isthmus method, in which two identical cylindrical capsules with secondary windings and soft iron end-plates formed a twin-isthmus in the 19.5 mm gap of an electromagnetic core of 51.6 mm×31.8 mm rectangular cross section. One capsule held the powder, the other neutralized the galvanometer throw due to the field alone. Calibration with empty capsules showed an influence of core remanence indicated by a lack of symmetry between the positive and negative fields corresponding to a given magnetizing current. This dissymmetry of the calibration curve is shown in the first columns in Tables I and II, which illustrate the method of determining coercive force of the powders, and, at the same time, present evidence for the statement that mere mechanical grinding increases the coercive force of a powder.

In Table I, fraction 2 was obtained from the original −150 +200-mesh fraction, by grinding in a 5-inch agate mortar to pass a 325-mesh sieve. This grinding required only a few minutes and was accomplished by sieving frequently and returning the oversize to the mortar, until the whole amount had passed the sieve; this short period of grinding increased the coercive force from 4.2 to 49.4 oersteds. Similarly, fractions 3, 4 and 5, having coercive forces of 18.4, 41.0 and 93.3 oersteds, respectively, differ only in a progressive degree of fineness, decreasing from the original −270 +350 mesh to the almost impalpable powder obtained by grinding the −325-mesh powder of fraction 4 in one-gram portions for 8 minutes each in the 5-inch agate mortar. In Table II, again, the three fractions differ only in a relative degree of fineness of

[3] A. Winkelmann, Handb. d. Physik, 2nd edition **5**, 213 (1908).

grain of about the same order as that of the series 3–4–5 of Table I, but here the original −80 +250-mesh artificial lodestone had a coercive force of 220 oersteds, which the two stages of further grinding increased to 245 and 271 oersteds, respectively.

The quantitative aspects of the relation between coercive force and mean grain size are exhibited in Tables III and IV, which give results respectively for ten sized fractions of the Hayden slag magnetite and for seven sized fractions of a natural magnetite from the Ural Mountains. The first four fractions in both cases were obtained by sieving the purified powder through standard sieves, the −350-mesh material being then further treated batchwise in an air-classifier to give respectively four and three air-sized fractions.

The coercive forces of Tables III and IV are plotted together against the corresponding mean diameters in microns in Fig. 1, and in Fig. 2 against "reciprocal microns" as an arbitrary scale for specific surface. The hyperbola $d(H_c-4)=467$ of Fig. 1 is drawn to correspond to the straight line $H_c=467(1/d)+4$ of Fig. 2 as an aid in estimating the deviations of the separate points from a linear relation between coercive force and specific surface. The straight line of Fig. 2 should go through the origin; it does not do so because the magnetites used had coercive forces in the massive state of about 2 and 6 oersteds, respectively, instead of zero. At these low fields where the points on the hysteresis curve are very closely spaced the error of interpolation was about 0.5–1.0 unit, so that the consistent deviations of the points above and below the hyperbola towards its horizontal end or of the straight line near the origin are errors caused by the residual magnetization, small for magnetites, of the samples used. On the vertical branch of the hyperbola the relatively large error of 5–10 units in coercive force, due to interpolation between points spaced far apart on the hysteresis curves at higher fields, is negligible compared to the large deviations caused by even a slight error in measuring grain size. See, for example, the last point on the straight line, for which two estimates of the mean diameter are entered in Fig. 2. Unfortunately, the mean diameter of the particles of a powder cannot be estimated with any precision, especially if the

TABLE III. *Purified artificial magnetite from Hayden slag.*

FRACTION	1 −100+150 mesh	2 −150+200 mesh	3 −200+270 mesh	4 −270+350 mesh	5	6	7	8	9	10
					−350 MESH, AIR-SEPARATED INTO FOUR FRACTIONS				BY GRINDING (2)	BY GRINDING (4)
PERCENT Fe_3O_4	91.5	91.3	93.1	94.9	98.2	93.1	92.6	86.2	91.3	94.9
PACKING DENSITY (g Fe_3O_4·cm^{-3})	2.58	2.43	2.55	2.70	2.85	2.75	2.42	1.85	2.40	2.76
$4\pi I$ (max. gauss at $H=2700$)	2484	2640	2721	2876	2915	2714	2445	1921	2539	2822
B_r (gauss)	22.7	25.7	70.2	142.5	166.4	178.6	316	462	307	619
H_c (oersted)	3.7	4.2	11.4	18.4	24.4	25.9	55.3	122	49.4	93.3
MEAN DIAMETER (microns)	180	134	92	40	20	18	9	3.5[a]	[b]	[c]

[a] Remeasured subsequently to be of mean diameter 4.2 microns.
[b] Measured after grinding to be 11 microns.
[c] Measured after grinding to be 4.7 microns.

TABLE IV. *Natural magnetite from the Ural Mountains.*

FRACTION	1 −100+150 mesh	2 −150+200 mesh	3 −200+270 mesh	4 −270+350 mesh	5	6	7
					−350 MESH, AIR-SEPARATED INTO THREE FRACTIONS		
PERCENT Fe_3O_4	97.5	97.9	97.9	97.5	96.7	95.3	91.6
PACKING DENSITY (g Fe_3O_4·cm^{-3})	2.71	2.67	2.63	2.52	2.74	2.47	1.71 2.28
$4\pi I$ (max. gauss at $H=2700$)	2849	2789	2743	2619	2825	2503	1691 2174
B_r (gauss)	51.6	77.6	94.5	144.4	220.1	397.3	438.6 547.3
H_c (oersted)	6.2	9.6	12.4	19.4	31.7	73.1	126.5 127.0
MEAN DIAMETER (microns)	180	134	92	40	18	9	3.7

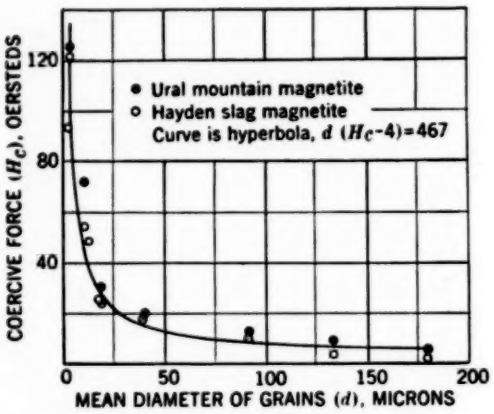

FIG. 1. Magnetite powders; variation of coercive force with grain size.

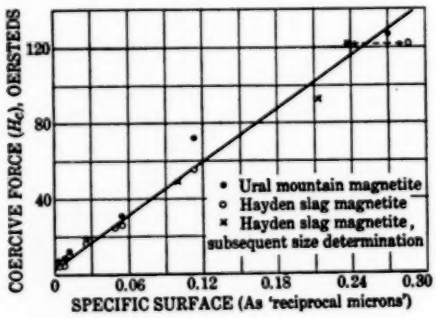

FIG. 2. Magnetite powders; variation of coercive force with specific surface.

particle sizes cover a considerable range[4] such as is the case in Tables III and IV with the finest air-sized fractions and the fractions obtained by further grinding. The error is least for powders sharply limited as to maximum and minimum particle size over a narrow range, but even then the absolute value of total surface would be more or less indefinite unless the particles were all of the same shape (spheres or cubes). Considering the difficulties and consequent large percentage error inherent in the measurement of grain size, the deviations of the points indicated in Figs. 1 and 2 are not regarded as excessive.

It remains only to show that no correction is needed for the variable packing densities at

[4] G. St. J. Perrott and S. P. Kinney, J. Am. Ceramic Soc. **6**, 417 (1923), where, in Table Ib, from estimates on the projected areas of nearly 200,000 particles of an unsized powder, the mean diameter is given as 3.0, 7.0, 21.0, or 36.4 microns, according to the method used for computing the mean.

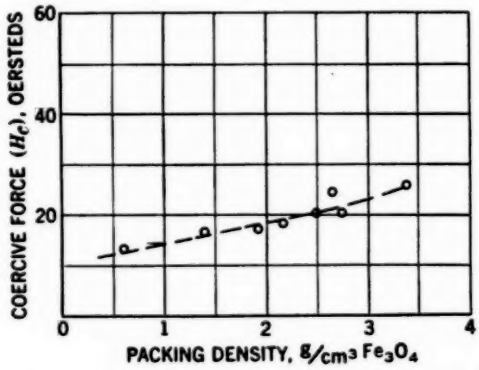

FIG. 3. Variation of coercive force with packing density.

which the coercive forces were measured. The entries for fraction 7 in Table IV are evidence for the insensitivity of coercive force to large variations of packing density, but since the error in H_c is large above 100 oersteds, an independent proof is given in Table V and Fig. 3. Here we present the coercive forces measured for one fraction of the Hayden slag magnetite at eight packing densities covering the range from 3.39 (g/cm^{-3}) Fe_3O_4 down to 0.61 g/cm^3 Fe_3O_4. The upper limit of density was attained by compressing the powder in a copper reinforced capsule; the lower limit, by mixing fraction 4 (Table III) with 75 percent of a -200-mesh magnetically inert powder. Clearly, the corrections for variable packing densities of Tables III and IV are within the experimental error of the coercive force measurements. It is interesting to note that the few widely-separated black grains of magnetite in the most dilute mixture of Table V still register such a large proportion of the coercive force characteristic of the compressed powder. C. W. Davis[5] has shown that coercive force does not change on orienting the particles of the powder.[5]

DISCUSSION OF RESULTS

A qualitative increase of coercive force with decreasing grain size has been known since 1916[6] and an extensive metallurgical literature on this subject now exists. But the first application of this fact to the fabrication of permanent magnets is due to R. S. Dean[7] who constructed his so-

[5] C. W. Davis, Physics **6**, 96 (1935).
[6] F. C. Thompson, Phil. Mag. **31** (6), 357 (1916).
[7] R. S. Dean, U. S. patent 1,904,859, issued April 18, 1933; filed March 24, 1930. Ferrous Alloy.

TABLE V. *Hayden slag magnetite, −270+350 mesh, at various packing densities.*

	IN COMPRESSED CYLINDERS			DILUTED WITH MAGNETICALLY INERT MATERIAL				
	Undiluted	5% inert	10% inert	5% inert	20% inert	30% inert	50% inert	75% inert
PACKING DENSITY (g $Fe_3O_4 \cdot cm^{-3}$)	3.39	2.77	2.50	2.66	2.18	1.94	1.40	0.61
$4\pi I$ (max. gauss at $H=2700$)	3675	3106	2993	2867	2272	2084	1488	724
B_r (gauss)	327	179	179	192	92	73	42	13
H_c (oersted)	25.8	20.5	20.4	24.1	18.1	17.0	16.6	13.5

called alpha-iron magnets by precipitating various fine dispersions in magnetically soft alpha-iron, free from carbon. The latest publication on permanent magnets of exceptionally high coercive force recognizes that all such magnets "are aggregates of numerous fine crystals separated from solid solution instead of being a solid solution; in other words, they are of a dispersed system."[8] This agrees with the dispersion theory of magnetic hardening[9] that has guided the magnetic work of the Bureau of Mines for some years.

The simple quantitative relation between coercive force and specific surface, revealed by Fig. 2, is believed to be new. This result, obtained with actual discrete particles, cannot be reconciled easily with elastic strain theories of coercive force, such for instance as that advocated by Kussmann and Scharnow[10] following a suggestion of McKeehan.[11] The existence of elastic strains at the points in the substance where the particles of the dispersed material are lodged cannot be doubted but in the light of the results of the present paper one must question the propriety of considering the elastic energy concerned as the cause of, or the measure of, coercive force.

The inadequacy of their elastic strain theory to account for the coercive force caused by free, discrete particles is admitted by Messkin and Kussmann[12] in the case of Nagaoka's[13] measurements on iron amalgams. The iron of the amalgams is now known to be present, not in solution, but as a suspension or dispersion of fine particles of metallic iron, which, by applying Stokes' law to the rate at which the iron particles rise in the mercury, have been shown[14] to vary in size from 2.62 microns down to below ultramicroscopic size, according to the current density at which the amalgams are made. If Nagaoka's amalgam containing 1.78 percent by weight, or 0.235 g/cm^{-3} of metallic iron, made at a current density of 12×10^{-3} amp. cm^{-2}, falls on Rabinowitsch and Zywotinski's curve connecting current density with mean diameter, the particles of metallic iron for which Nagaoka measured $H_c=240$ with $H_{max.}=3200$ (near the $H_{max.}=2700$ of Tables III, IV and V) would have had a mean diameter of 2.15μ. It is probably only a coincidence that $H_c=240$ is located at 1.95μ on extensions of the curves in Figs. 1 and 2 of the present paper. Messkin and Kussmann surmise that Nagaoka's high values for coercive force might be caused by surface forces on the particles of metallic iron; this suggestion could be interpreted in the case of ground magnetite powders, where the coercive force has proved to be directly proportional to specific surface, as supporting the theory that the energy expended in comminuting minerals and rocks is stored on, and proportional to, the surface of the particles. On the other hand, thorough search for this effect by painstaking thermochemical measurements[15] has consistently shown no difference in total surface energy before and after grinding, and therefore caution in accepting this explanation is advisable, at least until it is quite certain that the relation between

[8] K. Honda, H. Masumoto and Y. Shirakawa, *On New K. S. Permanent Magnet*, Sci. Rep. Tohoku **23**, 365 (1934).

[9] R. S. Dean, V. H. Gottschalk and C. W. Davis, *Magnetic Separation of Minerals*, Report of Investigations 3223, U. S. Bureau of Mines, February, 1934, pp. 3–13.

[10] A. Kussmann and B. Scharnow, "Ueber Koerzitivkraft. I. Teil Koerzitivkraft und mechanische Härte," Zeits. f. Physik **54**, 1 (1915); or, with more explicit detail, in the book, W. S. Messkin and A. Kussmann, *Die Ferromagnetischen Legierungen*, p. 109, Berlin, Julius Springer, 1932.

[11] L. W. McKeehan, Phys. Rev. **26**, 274 (1925).

[12] Reference 10, p. 121.

[13] H. Nagaoka, *Ueber verdünnte ferromagnetische Amalgame*, Wied. Ann. **59**, 66 (1896).

[14] M. Rabinowitsch and P. B. Zywotinski, *Quecksilber als Dispersions-mittel. Die Kolloide Natur der Eisenamalgame*, Kolloid Zeits. **52**, 31 (1930).

[15] C. G. Maier and C. T. Anderson, J. Chem. Phys. **2**, 513 (1934).

surface and coercive force is not a property of ferromagnetism itself.

That there is a relation between coercive force and grain size is implied also in some of the published data for hysteresis losses in ferrous metals. Thus, for example, the first series of magnetometric measurements of Sizoo[16] on wires of vacuum-fused electrolytic iron may be expressed to within 0.02 oersted by the equation $H_c = 0.038\ (1/d) + 0.39$, as shown in Table VI.

TABLE VI. *Sizoo's data for pure iron.*

GRAIN SIZE, d (mm)	11	7	6.3	2.7	1.2	0.7	0.6	0.3	0.1
COERCIVE FORCE, H_c									
Obs.	0.388	0.400	0.376	0.407	0.428	0.462	0.465	0.515	0.794
Calc.	0.394	0.395	0.396	0.404	0.422	0.445	0.454	0.517	0.771

The same type of equation, $H_c = 0.29(1/d) + 0.29$, roughly reproduces also the six values in Sizoo's first series of measurements on pure nickel,[17] as is shown in Table VII.

TABLE VII. *Sizoo's data for pure nickel.*

GRAIN SIZE, d (mm)	2	1.3	0.8	0.6	0.4	0.3
COERCIVE FORCE, H_c						
Obs.	0.45	0.55	0.58	0.70	1.07	1.26
Calc.	0.44	0.51	0.65	0.77	1.03	1.26

So, too, v. Auwers'[18] results on pure iron, obtained by use of the Koepsel permeameter, are fairly well expressed by the linear equation, $H_c = 0.05(1/d) + 0.40$, as indicated in Table VIII.

TABLE VIII. *von Auwers' data on pure iron.*

NO. OF GRAINS PER $mm^3 = (n)$	43.1	4.09	2.00	0.475	0.280	0.166
MEAN DIAMETER, $d = n^{-\frac{1}{3}}$ (mm)	0.15	0.50	0.71	1.45	1.89	2.45
H_c Obs.	0.75	0.60	0.48	0.45	0.45	0.35
H_c Calc.	0.73	0.60	0.47	0.43	0.43	0.42

Unfortunately the equation, $H_c = m(1/d) + c$, suggested by the results of the present paper, does not fit all published data on the variation of coercive force with grain size in ferrous alloys. However, recent summaries[19] of all work on the relation between hysteresis loss and grain size state that there is general agreement that, although other factors have greater influence, grain size does affect hysteresis loss and coercive force and that there is no satisfactory explanation for this effect.

The search for this effect was undertaken with powders of magnetite in the belief that electrostatic forces would cause a distribution of conduction electrons at the surface slightly different from that corresponding to equilibrium throughout the mass; and that, since magnetism is probably related to electron spin, this difference in electron distribution at the surface might conceivably be detected magnetically when the particles were so small that specific surface would become predominant. Conduction electrons are at present considered to have no influence on magnetic behavior, but a distortion of the lattice or a change in its spacing analogous to that calculated for a crystal of the NaCl type[20] might suffice to give a magnetic effect, because the 5-percent decrease in lattice spacing calculated by Lennard-Jones and Dent is confined almost entirely to the outside layer, and hence the ratio of disturbed to total electrons would increase proportionately with specific surface. To develop a theory of coercive force based on this explanation of the results of the present paper requires, among other things, a plausible mechanism by which such a surface anomaly would manifest itself as a coercive force rather than as a slight distortion of the normal magnetization curve.

[16] G. J. Sizoo, *Ueber den Zusammenhang zwischen Korngrösse und magnetischen Eigenschaften bei reinem Eisen*, Zeits. f. Physik **51**, 557 (1928).

[17] G. J. Sizoo, *Ueber den Zusammenhang zwischen Korngrösse und magnetischen Eigenschaften bei reinem Nickel*, Zeits. f. Physik **53**, 449 (1929).

[18] Otto von Auwers, *Ueber den Einfluss der Korngrösse auf die magnetischen Eigenschaften des Eisens*, Wiss. Veröff aus dem Siemens-Konzern **7**, Part 2, 197 (1929).

[19] T. D. Yensen, *Does Grain Size Influence the Magnetic Properties of Iron?* Metals and Alloys **1**, 493 (1930); Messkin and Kussmann, *Ferromagnetische Legierungen*, p. 330; G. E. Ruder, *The Influence of Grain Size on Magnetic Properties*. Trans. Am. Soc. Metals **22**, 1131, December (1934).

[20] J. E. Lennard-Jones and B. M. Dent, Proc. Roy. Soc. **A121**, 247 (1928).

The Propagation of Rayleigh Waves in Heterogeneous Media

CHAIM L. PEKERIS,* *Massachusetts Institute of Technology*

(Received February 11, 1935)

A method is given for obtaining a power series expansion in the wavelength for the Rayleigh wave velocity in a half-space whose density ρ and elastic constants λ and μ are functions of depth. This is followed by a discussion of the Rayleigh wave problem in media where $\lambda=\mu$ and $\mu(z)$ and $\rho(z)$ are special cases of the type $(\rho/\rho_0)=(\mu/\mu_0)=A\cosh^2(\alpha+\beta z)$.

I.

IN 1885 Rayleigh showed[1] that a homogeneous elastic medium can transmit waves whose amplitudes diminish exponentially with depth and whose velocity c, in terms of the shear wave velocity, is 0.9554 for an incompressible medium and 0.9194 for a medium where $\lambda=\mu$. These surface waves have a horizontal component u in the direction of propagation and a vertical component w. At the surface the ratio of the maximum amplitudes $(\bar{w}/\bar{u})_0$ is 1.47. Both c and $(\bar{w}/\bar{u})_0$ are independent of the wavelength L, but the variation of amplitudes with depth is given by exponentials of the form exp. $(-rz/L)$. Rayleigh waves appear as nearly harmonic oscillations on records of shallow earthquakes but $(\bar{w}/\bar{u})_0$ is usually less than 1.47. The harmonic character of the observed Rayleigh waves is attributed[2] to dispersion resulting from heterogeneity of the medium. The dispersion of Rayleigh waves in a medium composed of two homogeneous layers was studied by K. Sezawa[3] and T. Suzuki[4] who find that both c and $(\bar{w}/\bar{u})_0$ depend on the wavelength. Recently the subject of Rayleigh waves in layered media has been taken up by A. W. Lee[5] in connection with the interpretation of microseisms. Similar work on media with continuously varying properties is being done by R. Stoneley.[6] In the following we give a method of deriving an expression for c as a power series in L for any medium with continuously varying properties and later we treat the Rayleigh wave problem for several given media.

As a first step one is inclined to study the dispersing effect of small heterogeneity on Rayleigh waves. In doing so one soon finds the physically obvious fact that the degree of heterogeneity of a given medium depends on the wavelength considered, and that an appropriate measure of heterogeneity is the *relative* change of the density and elastic constants *within the space of a wavelength*. In the case of Rayleigh waves we know that in a homogeneous medium the depth to which the amplitudes are appreciable decreases steadily as the wavelength diminishes. We can therefore expect that in the limit of a vanishing wavelength c will be determined by the properties of the medium at the surface: in the expression

$$c=c_0+a_1L+a_2L^2+\cdots \qquad (1)$$

c_0 is $0.9554(\mu/\rho)_0^{\frac{1}{2}}$ for an incompressible medium and $0.9194(\mu/\rho)_0^{\frac{1}{2}}$ for a medium where $\lambda=\mu$. From dimensional considerations it is clear that a_1 is a linear function of $(1/p)(dp/dz)$, where p stands for any of the quantities ρ, λ and μ. Similarly a_2 is a linear function of $(1/p)(d^2p/dz^2)$ and of the squares and cross products of the terms appearing in a_1. With increasing wavelength the relative contribution of the high-order terms in (1) increases and the wave velocity becomes primarily determined by the properties of the medium at increasing depths. In the limit of infinite wavelengths c will be determined largely by the properties of the medium at infinite depths, or, what is equivalent to it, by the distribution of physical properties throughout the half-space. Formula (1) will, however, not always be valid for the entire range of wavelengths; we shall later see, in fact, that in some cases it has only a finite region of convergence.

* Fellow of the General Education Board.

[1] Lord Rayleigh, Proc. Lond. Math. Soc. **17**, 4 (1885).

[2] H. Jeffreys, *The Earth*, 2nd edition, p. 94, 1929.

[3] K. Sezawa, Tokyo, Bull. Earthquake Res. Institute **3**, 16 (1927); K. Sezawa and K. Kanai, Bull. Earthquake Res. Institute **12**, 263 (1934).

[4] T. Suzuki, Bull. Earthquake Res. Institute **11**, 187 (1933).

[5] A. W. Lee, M. N. R. A. S. Geophys. Supp. **3**, 238 (1934).

[6] R. Stoneley, Geophys. Supp. **3**, 222 (1934); See also H. Honda, Geophys. Mag. **4**, 137 (1931).

II.

Consider the two-dimensional motion of a half-space whose density ρ and elastic constants μ and λ are given functions of z. The equations of motion

$$\rho\frac{\partial^2 u}{\partial t^2}=\frac{\partial}{\partial x}\left(\lambda\delta+2\mu\frac{\partial u}{\partial x}\right)+\frac{\partial}{\partial y}\left[\mu\left(\frac{\partial v}{\partial x}+\frac{\partial u}{\partial y}\right)\right]+\frac{\partial}{\partial z}\left[\mu\left(\frac{\partial w}{\partial x}+\frac{\partial u}{\partial z}\right)\right], \tag{2}$$

$$\rho\frac{\partial^2 w}{\partial t^2}=\frac{\partial}{\partial z}\left(\lambda\delta+2\mu\frac{\partial w}{\partial z}\right)+\frac{\partial}{\partial x}\left[\mu\left(\frac{\partial u}{\partial z}+\frac{\partial w}{\partial x}\right)\right]+\frac{\partial}{\partial y}\left[\mu\left(\frac{\partial v}{\partial z}+\frac{\partial w}{\partial y}\right)\right] \tag{3}$$

reduce under the assumption

$$u\equiv\partial F/\partial x,\quad F=f(z)e^{ik(x-ct)},\quad w=\psi(z)e^{ik(x-ct)},\quad v=0 \tag{4}$$

to

$$k^2c^2lf+\ddot{f}-k^2(\gamma+2)f+(1+\gamma)\dot{\psi}+\beta(\psi+\dot{f})=0, \tag{5}$$

$$k^2c^2l\psi+(\gamma+2)\ddot{\psi}-k^2(\gamma+1)\dot{f}-k^2\psi+(\dot{\gamma}+\gamma\beta)(\dot{\psi}-k^2f)+2\beta\dot{\psi}=0, \tag{6}$$

where $\gamma\equiv\lambda/\mu$, $\beta\equiv\dot{\mu}/\mu$, $l\equiv\rho/\mu$.[7]

The boundary conditions for free vibrations are that the stresses shall vanish at the surface and at infinity:

$$ik\mu(\psi+\dot{f})=0,\quad(\lambda+2\mu)\dot{\psi}-\lambda k^2f=0\qquad\text{at } z=0 \text{ and } z=\infty. \tag{7}$$

Since $k=2\pi/L$, the solutions of (5) and (6) which lead to the development (1) are the asymptotic solutions for large values of k.

Let

$$f=\exp\left[-k\int^z m(z)dz\right]U(z),\qquad \psi=-k\exp\left[-k\int^z m(z)dz\right]S(z),$$

substitute in (5) and (6) obtaining

$$k^2[c^2lU+(m^2-\gamma-2)U+(1+\gamma)mS]+k[-\dot{m}U-2m\dot{U}-\beta mU-\beta S-(1+\gamma)\dot{S}+\ddot{U}+\beta\dot{U}]=0, \tag{8}$$

$$k^2[c^2lS+m^2(\gamma+2)S-S-(\gamma+1)mU]+k[-(\gamma+2)\dot{m}S-2m\dot{S}(\gamma+2)-(\dot{\gamma}+\gamma\beta+2\beta)mS$$
$$+(\gamma+1)\dot{U}+(\dot{\gamma}+\gamma\beta)U]+[(\gamma+2)\ddot{S}+(\dot{\gamma}+\gamma\beta+2\beta)\dot{S}]=0. \tag{9}$$

Further, assume

$$U(z)=U_0(z)+(1/k)U_{-1}(z)+\cdots,\qquad S(z)=S_0(z)+(1/k)S_{-1}(z)\cdots. \tag{10}$$

We now proceed to compute the coefficients c_0, $c_{-1}\cdots$ in an expansion

$$c^2=c_0+(1/k)c_{-1}+\cdots \tag{11}$$

for the desired Rayleigh wave velocity, c. Substitute in (8) and (9) and equate the coefficients of each power of k to zero. The coefficients of k^2 yield the relations:

$$U_0[c_0l+m^2-\gamma-2]+(1+\gamma)mS=0,\qquad U_0[-m(\gamma+1)]+S_0[c_0l+m^2(\gamma+2)-1]=0, \tag{12}$$

implying that

$$[c_0l+m^2-\gamma-2][c_0l+m^2(\gamma+2)-1]+(1+\gamma)^2m^2=0, \tag{13}$$

for all values of z, the roots of which are $\pm(1-c_0l)^{\frac{1}{2}}$ and $\pm(1-c_0l/(\gamma+2))^{\frac{1}{2}}$. To each root there corresponds a solution for U and S (f and ψ) which is obtained by substituting the given root for m

[7] Eqs. (5) and (6) are valid also for a cylindrical wave if we define u_r as $\partial F/\partial r$ and change the exponential in (4) to $e^{-ikct}H_0^{(1)}(kr)$. See Physics **5**, 312 (1934).

in (8) and (9) and determining successively the functions in the development (10) by annulling the coefficients of each power of k. We shall see later that the condition for the vanishing of the stresses at the surface determines a value for c_0 such that the roots are real at the surface. Let $m_1(z) \equiv +(1-c_0 l)^{\frac{1}{2}}$, $m_2(z) \equiv +(1-c_0 l/(\gamma+2))^{\frac{1}{2}}$, m_1 and m_2, then, being positive in a certain region close to the surface, and denote the corresponding solutions for U and S by P, Q and R, T, respectively. The appropriate solutions for f and ψ will then be the combinations

$$f = \exp\left[-k\int^z m_1(z)dz\right]P(z) + \exp\left[-k\int^z m_2(z)dz\right]Q(z), \tag{14}$$

$$\psi = -k\exp\left[-k\int^z m_1(z)dz\right]R(z) - k\exp\left[-k\int^z m_2(z)dz\right]T(z), \tag{15}$$

where

$$P(z) = P_0(z) + (1/k)P_{-1}(z) + \cdots, \qquad Q(z) = Q_0(z) + (1/k)Q_{-1}(z) + \cdots, \tag{16}$$

with similar expansions for $R(z)$ and $T(z)$. It follows from Eq. (12) that

$$R_0(z) = P_0(z)/m_1(z), \qquad T_0(z) = m_2(z)Q_0(z). \tag{17}$$

The boundary conditions (7) at the surface become

$$\dot{P} + \dot{Q} = k(R + T + m_1 P + m_2 Q), \tag{18}$$

$$\dot{R} + \dot{T} = k[m_1 R + m_2 T - (P+Q)\gamma/(\gamma+2)], \qquad \text{at } z=0 \tag{19}$$

to be satisfied identically in k. The coefficients of k in (18) and (19), when equated to zero, give in conjunction with (17) the relations

$$[m_1 + (1/m_1)]P_0 + 2m_2 Q_0 = 0, \qquad [1-\gamma/(\gamma+2)]P_0 + [m_2^2 - \gamma/(\gamma+2)]Q_0 = 0. \tag{20}$$

By making the determinant of the coefficients in (20) vanish, we obtain an equation determining c_0:

$$4m_1 m_2 = (m_1^2+1)^2, \tag{21}$$

where m_1 and m_2 have their values at the surface. (21) is identical with the equation determining the Rayleigh wave velocity in a homogeneous medium having the properties of the skin layer. It now follows from (20) that

$$Q_0 = -P_0(m_1^2+1)/2m_1 m_2, \qquad T_0 = -P_0(m_1^2+1)/2m_1, \qquad \text{at } z=0, \tag{22}$$

in contradistinction to relations (17) which are valid for all values of z. The annulling of the coefficients of k in (8) and (9) now gives the differential equations

$$\dot{P}_0/P_0 = (lc_{-1}/2m_1) - (\beta/2) - \dot{m}_1(m_1^2+1)/2m_1(m_1^2-1), \tag{23}$$

$$\dot{Q}_0/Q_0 = lc_{-1}/(2m_2\gamma + 4m_2) + \dot{m}_2(3m_2^2-1)/(2m_2 - 2m_2^3) - (2\beta + \dot{\gamma} + \gamma\beta)/(2\gamma+4), \tag{24}$$

which is conjunction with (17) determine also R_0 and T_0. We thus get, to within terms of the order of $(1/k)$ in (16),

$$f = \exp\left[-k\int_0^z m_1 dz\right]\left\{(m_1/\rho)^{\frac{1}{2}}\exp\left[\frac{c_{-1}}{2}\int_0^z (l/m_1)dz\right]\right\}$$

$$+\exp\left[-k\int_0^z m_2 dz\right]\left\{(m_2\rho)^{-\frac{1}{2}}\exp\left[\frac{c_{-1}}{2}\int_0^z [l/m_2(\gamma+2)]dz\right]\right\}, \tag{25}$$

$$\psi = -k \exp\left[-k\int_0^z m_1 dz\right]\left\{(m_1\rho)^{-\frac{1}{2}} \exp\left[\frac{c_{-1}}{2}\int_0^z (l/m_1)dz\right]\right\}$$

$$-k \exp\left[-k\int_0^z m_2 dz\right]\left\{(m_2/\rho)^{\frac{1}{2}} \exp\left[\frac{c_{-1}}{2}\int_0^z [l/m_2(\gamma+2)]dz\right]\right\}. \quad (26)$$

With $u = ikfe^{ik(x-ct)}$, $w = \psi e^{ik(x-ct)}$ these give for $|\bar{w}/\bar{u}|_0$ the value $(m_2/m_1)_0^{\frac{1}{2}} = 1.47$, its value for a homogeneous medium of the properties of the skin layer. This is the first order approximation to the solutions of (5) and (6) for the limiting case of vanishing wavelengths. (25) and (26) are valid for media where the P and S-wave velocities are non-decreasing functions of depth. For, in such media both m_1 and m_2 stay real and, no matter what the sign of c_{-1} may be, the first exponentials will insure—in the limit of large k—the vanishing of the stresses at infinity. In media where the velocities decrease with depth throughout or in certain regions, the appropriate solutions will in general be combinations of all of the four particular solutions of (5) and (6), some of which will be oscillatory. The state of motion will then resemble the propagation of bodily waves rather than surface waves, and the stresses will not vanish at infinity. If, however, at great depth the velocities eventually increase again, the motion will there be represented by solutions of the type of (25) and (26) and the stress-condition will be satisfied. In what follows we shall assume that the medium is capable of transmitting Rayleigh waves.

If we now use the k^0 terms in (18) and (19), we obtain a linear equation for the determination of c_{-1}:

$$lc_{-1}\left[\frac{3m_1^2-1}{2m_1^3} - \frac{2}{(m_1^2+1)m_2(\gamma+2)}\right] = \beta\left[\frac{1}{2} + \frac{m_2(\gamma+2)}{m_1(\gamma+1)} - \frac{(m_1^2+1)(\gamma+2)-1+\gamma}{2m_1^2(\gamma+1)} - \frac{2}{(m_1^2+1)(\gamma+1)}\right]$$

$$+\dot{m}_1\left[\frac{(m_1^2-1)}{2m_1^3} - \frac{2-(m_1^2+1)(\gamma+2)}{(m_1^2-1)(\gamma+1)m_1}\right] + \dot{m}_2\left[-\frac{2m_2^2(\gamma+2)}{m_1(\gamma+1)(1-m_2^2)} + \frac{2(3m_2^2-1)+2(\gamma+2)(1-m_2^2)}{m_2(m_1^2+1)(1-m_2^2)(1+\gamma)}\right]$$

$$+\dot{\gamma}\left[-\frac{2}{(m_1^2+1)(\gamma+2)(\gamma+1)} + \frac{m_2}{m_1(\gamma+1)}\right], \quad (27)$$

where, as before, m_1, m_2, γ and their derivatives have their values at the surface. In particular, for the case $\lambda = \mu(\gamma = 1)$ (27) reduces to

$$lc_{-1} = 0.5373\beta - 1.534(\dot{l}/l), \quad (28)$$

while the corresponding relation for an incompressible medium ($\gamma = \infty$) is

$$lc_{-1} = 0.5640\beta - 2.108(\dot{l}/l). \quad (29)$$

(29) agrees with Eq. (30) of Stoneley's paper[6] (if we insert in the latter $\delta q/q$ for $\delta c/c$). I have checked (28) and (29) by an independent calculation in which I started with the solutions for a homogeneous medium and treated the first order heterogeneity in ρ, λ and μ as a perturbation. We shall also have occasion to verify (28) in the following section.

We can now proceed with the determination of c_{-2}. The algebra is rather involved, but the result is a linear relation for c_{-2} with a right-end side which is linear in the second derivatives of ρ, λ and μ and the products of their first derivatives. Similarly it is possible to determine the other terms in (11). It should be noticed that the dimensional considerations mentioned above reveal the structure of the coefficients c_{-1} in Eq. (11) except for numerical coefficients which are independent of the medium. We can therefore determine these coefficients once and for all if we succeed in obtaining an expression for the wave velocity in a given medium. Thus from the examples treated in the following section (Eqs. (3.9) and (3.10)), I find that, when $\gamma = 1$,

$$lc_{-2}=1.433\dot{\beta}+0.2167\beta^2+A\beta(\dot{l}/l)+B(\ddot{l}/l)+C(\dot{l}/l)^2.$$

The coefficients A, B and C remain undetermined because in the above examples $l=$constant.

III.

In the following we shall assume that $\lambda=\mu$ $(\gamma=1)$, this being nearly realized in the earth's crust. Further, let $f\equiv H/(\mu)^{\frac{1}{2}}$, $\psi\equiv G/(\mu)^{\frac{1}{2}}$, then Eqs. (5) and (6) reduce to the convenient forms

$$\ddot{H}+[k^2xl-(\ddot{\mu}/2\mu)+(\dot{\mu}/2\mu)^2-3k^2]H+2\dot{G}=0, \tag{3.1}$$

$$3\ddot{G}+[k^2xl-(3\ddot{\mu}/2\mu)+\tfrac{3}{4}(\dot{\mu}/\mu)^2-k^2]G-2k^2\dot{H}=0, \tag{3.2}$$

where we have denoted c^2 by x. If we assume $l=$constant, then the terms in brackets in (3.1) and (3.2) will be independent of z provided

$$\tfrac{1}{2}(\ddot{\mu}/\mu)-\tfrac{1}{4}(\dot{\mu}/\mu)^2=\beta^2, \tag{3.3}$$

β being a constant.[8] The solution of (3.3) is, $\mu=C\cosh^2(\alpha+\beta z)$, C and α being arbitrary constants. With

$$b\equiv\beta/k, \qquad r\equiv[1+b^2-(2x/3)-(1/3)(x^2-12b^2)^{\frac{1}{2}}]^{\frac{1}{2}}, \qquad s\equiv[1+b^2-(2x/3)+(1/3)(x^2-12b^2)^{\frac{1}{2}}]^{\frac{1}{2}} \tag{3.4}$$

one finds that (3.1) and (3.2) are satisfied by

$$f=[Ae^{-krz}+Be^{-ksz}]/\cosh(\alpha+\beta z),$$

$$\psi=k\{(A/r)[x-6-(x^2-12b^2)^{\frac{1}{2}}]e^{-krz}+(B/s)[x-6+(x^2-12b^2)^{\frac{1}{2}}]e^{-ksz}\}/6\cosh(\alpha+\beta z). \tag{3.5}$$

The boundary conditions (7) at the surface require that

$$\{[x-6-(x^2-12b^2)^{\frac{1}{2}}]-6r(r+b\cdot\operatorname{tgh}\alpha)\}\cdot\{3[x-6+(x^2-12b^2)^{\frac{1}{2}}](s+b\cdot\operatorname{tgh}\alpha)+6s\}$$
$$=\{[x-6+(x^2-12b^2)^{\frac{1}{2}}]-6s(s+b\cdot\operatorname{tgh}\alpha)\}\cdot\{3[x-6-(x^2-12b^2)^{\frac{1}{2}}](r+b\cdot\operatorname{tgh}\alpha)+6r\}. \tag{3.6}$$

In virtue of (3.4), (3.6) reduces to an identity if we make

$$(r+b\cdot\operatorname{tgh}\alpha)(s+b\cdot\operatorname{tgh}\alpha)=1/3, \tag{3.7}$$

an equation for the determination of x as a function of b and α. The root (3.7) of (3.6) is the proper one since it gives the right expression for x when $b=0$. From (3.7) we now get

$$x^4-8x^3(1+b^2-b^2v^2)+x^2[(64/3)+b^2(52-48v^2)+22b^4(1-v^2)^2]$$
$$-x\{(8+8b^2-8b^2v^2)[(10/3)+b^2(10-8v^2)+3b^4(1-v^2)^2]-(16/3)(1+b^2)\}+(64/9)$$
$$+(160b^2/3)(1-v^2)+b^4(116-84v^2)(1-v^2)+6b^6(10-8v^2)(1-v^2)^2+9b^8(1-v^2)^4=0, \tag{3.8}$$

where $v\equiv\operatorname{tgh}\alpha$. The relevant root of (3.8) can be obtained in closed form in the limiting cases of $v=0$ and $v=1$, corresponding to $(\mu/\mu_0)=\cosh^2\beta z$ and $(\mu/\mu_0)=e^{2\beta z}$, respectively. We have for $v=0$:

$$x=2(1+b^2)-(b^4-2b^2+4/3)^{\frac{1}{2}} \tag{3.9}$$

and for $v=1$:
$$b^2=[(16/3)(1/3-x+x^2)-2x^3+x^4/4]/[(8x/3)-x^2]. \tag{3.10}$$

In each case x starts with the value 0.8453 for $b=0$, but as $b\to\infty$, it approaches the limit (8/3) for $v=1$, while for $v=0$ it becomes infinite as b^2. This difference of behavior for large values of b (wavelengths) can be obtained directly from (3.8), the relevant root becoming asymptotically $b^2(1-v^2)$.[9]

[8] This constant β should not be confused with the variable $\beta(z)\equiv\dot{\mu}/\mu$ of section II.

[9] The asymptotic behavior of x and $|\bar{w}/\bar{u}|_0$ for long wavelengths (small k) can be studied directly from (5) and (6), whereby the above results are verified.

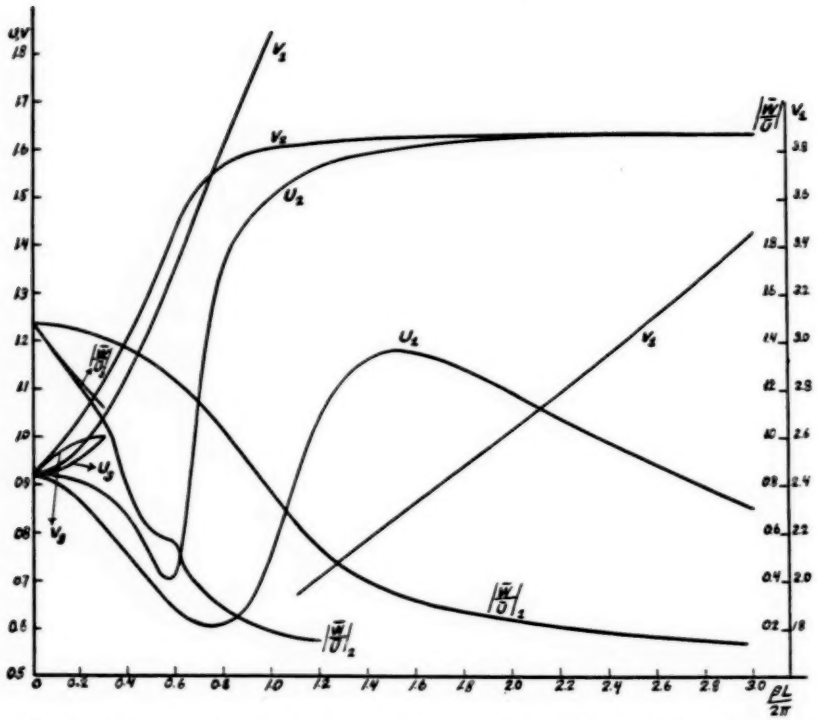

FIG. 1. Rayleigh wave velocities and surface amplitude-ratios in media 1, 2 and 3, in which $\lambda=\mu$ and $(\rho/\rho_0)=(\mu/\mu_0)=(\lambda/\lambda_0)=\cosh^2\beta z$, $e^{2\beta z}$, $(1+\beta z)^2$, respectively. v and u denote the Rayleigh wave velocity and group velocity in units of the shear wave velocity at the surface. $|\bar{w}/\bar{u}|$ denotes the absolute value of the ratio of the vertical to the horizontal amplitudes at the surface. Note that in medium (3) Rayleigh waves of wavelength $L>0.2989(2\pi/\beta)$ cannot exist.

In Fig. 1 we have plotted the wave velocity $c=x^{\frac{1}{2}}$ and the group velocity $u=x^{\frac{1}{2}}[1-(b/2x)(dx/db)]$, for $v=1$ and for $v=0$. We have also plotted in each case the absolute values of $(\bar{w}/\bar{u})_0$ which are given by

$$|\bar{w}/\bar{u}|_0=|[(s+r)(3+b^2-x)+b\ \text{tgh}\ \alpha(3+b^2-x+sr)]/(3+b^2-x-sr)|. \tag{3.11}$$

It is seen that the latter start with the value 1.47 for a homogeneous medium and decrease in a monotone fashion to zero with increasing wavelength or heterogeneity. The increase in wave velocity with wavelength seems to be in accord with the observed character of Rayleigh waves, which in many cases consist of a group of periodic oscillations of long wavelength followed by a group of decidedly shorter wavelength.

One other medium which is a solution of (3.3) is worthy of notice. If in the solution $\mu=\mu_0\sinh^2[\alpha(1+\beta z)]/\alpha^2$ we let $\alpha\to 0$, we get $(\mu/\mu_0)=(1+\beta z)^2$. The equation for the wave velocity can be obtained directly from (3.7) by writing cotgh α for tgh α. Thus, with $d\equiv\beta/k$,

$(d+r)(d+s)=\frac{1}{3}$, or

$$d=-\{[\tfrac{1}{2}-(x/3)+\tfrac{1}{2}[(1-x)(1-x/3)]^{\frac{1}{2}}\}^{\frac{1}{3}}+\{(5/6)-(x/3)-\tfrac{1}{2}[(1-x)(1-x/3)]^{\frac{1}{2}}\}^{\frac{1}{3}}.^{10} \tag{3.12}$$

d, again, starts with the value zero for $x=0.8453$ and increases to 0.2989 for $x=1$, as is shown in Fig. 1. For larger values of x, d and with it k become complex, which precludes the existence of free progressive waves. With a given medium(β) of the above type there is, therefore, a maximum wavelength above which no Rayleigh waves can exist.

I am indebted to Professor L. B. Slichter for helpful suggestions during the preparation of this paper.

[10] (3.12) and (3.10) are in agreement with (28).

A Note on a Problem in Conduction

L. B. SNODDY, *University of Virginia*

(Received February 13, 1935)

The expression for the temperature distribution in a semi-infinite bar with heat supplied to the surface $x=0$ at a rate given by $H=kt^n (n=0, 1, 2\cdots)$ is derived, assuming no radiation to the surrounding medium and an initial temperature of zero. Curves are given which enable the distribution in a bar of any material to be readily computed for $n=0$ and $n=1$. The solution serves equally well to determine the voltage variation in a semi-infinite non-inductive cable with entering current proportional to t^n provided the heat constants are replaced by the appropriate electrical parameters.

DURING a study of electrode heating in certain types of electrical discharges it became necessary to compute the temperature distribution with a heat input at the electrode surface proportional to the time. To make this investigation of more general interest the electrode was assumed to be in the form of a semi-infinite bar with no radiation to the surrounding medium, an initial temperature of zero and a rate of heat input (at the end $x=0$) given by $H=kt^n$ $(n=0, 1, 2\cdots)$.

The distribution for heat supplied to the end at a constant rate $(n=0)$ has been worked out in detail by Wright.[1] General methods for the solution of all problems of this kind are available. Each case, however, involves considerable computational labor so it was thought worthwhile to publish these results in the hope that they might be of use in some other investigation. The solution serves equally well for the determination of the voltage variation in a semi-infinite non-inductive cable with an entering current proportional to t^n, provided the heat constants are replaced by the appropriate electrical parameters.

Using the Heaviside notation, the temperature distribution is determined by the operational equation[2]

$$u(t, x)=(1/K\rho c p)^{\frac{1}{2}}e^{-2(\lambda p)^{\frac{1}{2}}}H(p) \qquad (1)$$

or by the integral equation

$$(1/K\rho c)^{\frac{1}{2}}e^{-2(\lambda p)^{\frac{1}{2}}}H(p)/p^{\frac{1}{2}}=\int_0^\infty u(t)e^{-pt}dt \qquad (2)$$

where K is the heat conductivity, ρ the density, c the specific heat and λ is written for $x^2\rho c/4K$.

With $H(t)(=kt^n)$ given, $H(p)$ is defined by the integral[2]

$$\int_0^\infty kt^n e^{-pt}dt=kn!/p^{n+1}=H(p)/p.$$

Inserting this value of $H(p)$ in (2), it is found from a table of integrals that the variation of temperature at the surface $x=0$ (i.e., $\lambda=0$) is given by

$$u(t, 0)=\frac{kn!}{(K\rho c\pi)^{\frac{1}{2}}}\frac{2^{n+1}t^{n+\frac{1}{2}}}{1\cdot 3\cdot 5\cdots(2n+1)}. \qquad (3)$$

After substituting for $H(p)$ in Eq. (1), the variation along the bar can be expressed in the form

$$u(t, x)=\frac{kn!}{(K\rho c)^{\frac{1}{2}}}\frac{p^{\frac{1}{2}}}{p^{n+1}}e^{-2(\lambda p)^{\frac{1}{2}}}.$$

Introducing the two functions

$$u_1=[k/(K\rho c)^{\frac{1}{2}}]p^{\frac{1}{2}}e^{-2(\lambda p)^{\frac{1}{2}}}$$
$$=[k/(K\rho c\pi)^{\frac{1}{2}}]e^{-\lambda/t}/t^{\frac{1}{2}}, \qquad (4)$$

$$u_2=n!/p^{n+1}=t^{n+1}/n+1, \qquad (5)$$

the distribution is obtained from the equation[3]

$$u(t, x)=d/dt\int_0^t u_2(t-z)u_1(z)dz.$$

Using the values of u_1 and u_2 defined by (4) and (5), carrying out the indicated differentiation and replacing z by λw this becomes

$$u(t, x)=\frac{k}{(K\rho c\pi)^{\frac{1}{2}}}\lambda^{n+\frac{1}{2}}\int_0^{t/\lambda}(t/\lambda-w)^n e^{-1/w}/w^{\frac{1}{2}}dw$$

or, abbreviating

$$u(t, x)=[k/(K\rho c\pi)^{\frac{1}{2}}]\lambda^{n+\frac{1}{2}}F_n(t/\lambda). \qquad (6)$$

[1] C. E. Wright, Phil. Mag. [7] **12**, 1015 (1931).

[2] John R. Carson, *Electric Circuit Theory and Operational Calculus*, McGraw-Hill (1926), pp. 48 and 51.

[3] Reference 2, p. 44.

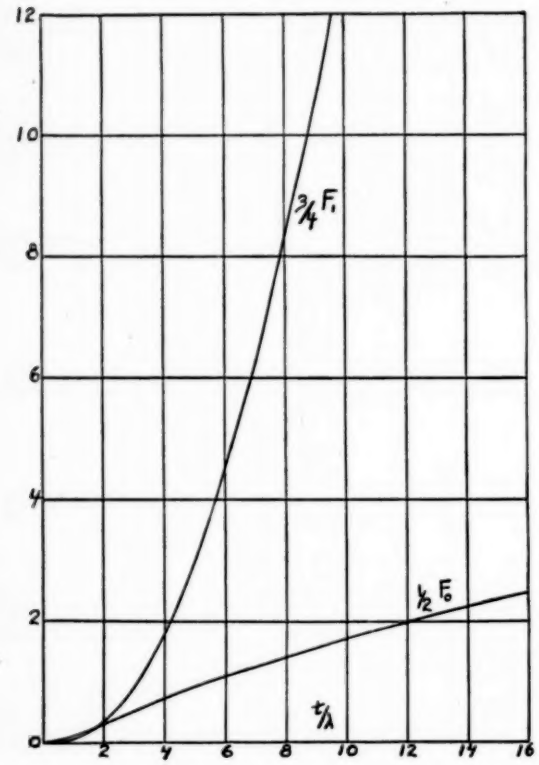

FIG. 1. Graphs of the function F_n for $n=0$ and $n=1$ occurring in the equation $u=[k/(K\rho c)^{\frac{1}{2}}]\lambda^{n+\frac{1}{2}}F_n(t/\lambda)$, giving the temperature distribution in a semi-infinite bar with heat supplied to the end at a rate $H=kt^n$. λ is written for $x^2\rho c/4K$.

F_n for any particular case is readily obtained in a form suitable for computation by repeated integration by parts remembering that

$$\int_0^{t/\lambda} e^{-1/w}/w^{\frac{1}{2}}dw=\pi^{\frac{1}{2}}[1-\text{erf }(\lambda/t)^{\frac{1}{2}}].$$

F_0 and F_1 are given below.

$$F_0=2[(t/\lambda)^{\frac{1}{2}}e^{-\lambda/t}-\pi^{\frac{1}{2}}(1-\text{erf }(\lambda/t)^{\frac{1}{2}})],$$

$$F_1=(4/3)[(t/\lambda)^{\frac{1}{2}}e^{-\lambda/t}(t/\lambda+1)-\pi^{\frac{1}{2}}(3t/2\lambda+1)(1-\text{erf }(\lambda/t)^{\frac{1}{2}})].$$

TABLE I. *Values of the functions* $\frac{1}{2}F_0$ *and* $\frac{3}{4}F_1$ *for different values of* t/λ.

t/λ	$\frac{1}{2}F_0$	$\frac{3}{4}F_1$	t/λ	$\frac{1}{2}F_0$	$\frac{3}{4}F_1$
0.5	0.0151	0.0025	6	1.07	4.52
0.8	0.0544	0.0171	7	1.24	6.27
1	0.0891	0.0388	8	1.40	8.24
2	0.295	0.324	9	1.55	10.46
3	0.507	0.925	10	1.70	12.90
4	0.708	1.84	16	2.47	31.81
5	0.896	3.04	20	2.90	48.02

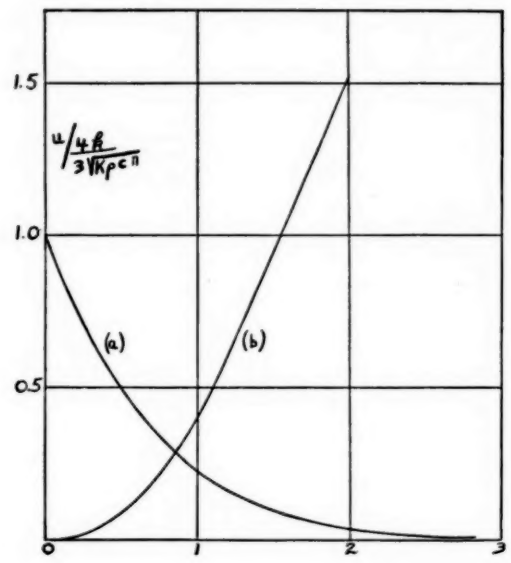

FIG. 2. Plot of temperature distribution in a semi-infinite bar with heat supplied at a rate $H=kt$. For this bar $(K/\rho c)^{\frac{1}{2}}$ was taken as unity: (a) At 1 sec. after start of heating showing the variation with distance from end of bar; (b) at a distance $(0.4)^{\frac{1}{2}}$ cm from the input end showing the variation with time.

The functions $\frac{1}{2}F_0$ and $\frac{3}{4}F_1$ for different values of t/λ are given in Table I and are shown graphically in Fig. 1. Since $\lambda=x^2\rho c/4K$ it is a simple process, using these curves, to plot the temperature distribution along a bar at any given time or the variation with respect to the time at any given position ($x>0$; for $X=0$ the temperature is determined from Eq. (3)). This is illustrated in Fig. 2 for $n=1$, i.e., a rate of heat input proportional to the time. In (a) the temperature is shown as a function of distance after 1 sec. of heating and in (b) as a function of time at a point $(0.4)^{\frac{1}{2}}$ cm from the input end. For this purpose $(K/\rho c)^{\frac{1}{2}}$ was taken to be unity. It happens that this is approximately the value for copper.

The total amount of heat added to the bar at any instant can be obtained from (6) since

$$W\text{ (total heat)}=\rho c\int_0^\infty u(t,x)dx.$$

It is easily verified that the value of this integral is $kt^{n+1}/n+1$ as it should be with a rate of heat input given by kt^n.

Internal Dissipation in Solids for Small Cyclic Strains

R. L. WEGEL AND H. WALTHER, *Bell Telephone Laboratories*

(Received February 2, 1935)

This paper presents the results of investigations of dissipation of energy in vibrating solids, mostly metals, by means of longitudinal and torsional vibrations of cylindrical rods. The amplitudes of strain used have been kept between 10^{-5} cm/cm and 10^{-8} cm/cm, in which range the dissipation of energy is proportional to the square of the strain. The specific dissipative property of a material is expressed in three different ways: (1) Equivalent viscosity or the ratio of stress to dissipative component of strain rate; (2) hysteretic constant defined as the area in ergs of the cyclic stress-strain diagram; and (3) elastic phase constant defined as the ratio of specific elastic reactance to equivalent viscosity. Within a range of frequencies 100 to 100,000 cycles per second the results show that the hysteretic constant is proportional to some power Δ of the frequency, the numerical value of the exponent Δ varying between the limits $-\frac{1}{3}$ and $+\frac{1}{3}$, depending on the kind of material and its internal structural condition. Measurements made with longitudinal and torsional vibration indicate that dissipation is associated with dilatation as well as with pure shear. Preliminary studies are described showing the correlation between internal dissipation in metals and temperature hardness effects of annealing and aging.

INTRODUCTION

A CONSIDERABLE quantity of data has accumulated during the past hundred years on the dissipation of energy resulting from distortion in solids. The process of this conversion of energy in a solid is usually known as elastic hysteresis. It appears to be principally determined by the magnitude of the strain rather than its velocity. In contrast, the analogous mechanism in a fluid, which is known as viscosity, is principally dependent on the strain rates, or more specifically—the shear rates. The results given in this paper are interpreted to show, in a solid, that although dissipation appears to be principally dependent on strain it is also in varying degrees determined by the strain rate.

It is well known that in plastic flow the magnitude and other parametric characteristics of internal dissipation vary in a given solid with the amount of the deformation and with the rate of deformation. That this is also true, though in a different way, for vanishingly small strains seems not to be so generally recognized. When a measurement of internal dissipation is made in a specified way, over a range of sufficiently small strains the law giving this dissipation as a function of strain amplitude does not change. Over this range of "small" strains, the process of application of the strain used to measure dissipation does not change the gross mechanical properties of the solid by any appreciable amount. As the test strain is increased above this range, the constant "small" strain law is gradually departed from more and more until the limiting violent deformation resulting from the test strain, is reached where plastic flow or rupture takes place. Care has been taken in the work reported here to make all measurements safely in the small cyclic strain range of 10^{-5} to 10^{-8} cm/cm in the frequency range 10^{-2} to 10^{5} cycles per second. It seems probable that some of the published results apply to test strains in the transition range between "small" and "large" strains and that failure adequately to specify experimental conditions has contributed a certain amount of confusion.

Of the common experimental procedures, the torsion pendulum and resonant rod methods were investigated and the second found most readily productive of the kind of result desired. A technique was therefore devised for obtaining the internal dissipation in a cylindrical bar at the various frequencies of its series of natural resonances, both for longitudinal and for torsional vibration.

EXPERIMENTAL PROCEDURE AND CALCULATION OF MATERIAL CONSTANTS

Apparatus

Fig. 1 is a schematic diagram of the set-up for measuring the resonant characteristics of a bar. The bar B is usually supported at its center at C_1-C_2. This suspension consists of a frame with four pegs placed at the corners of a square

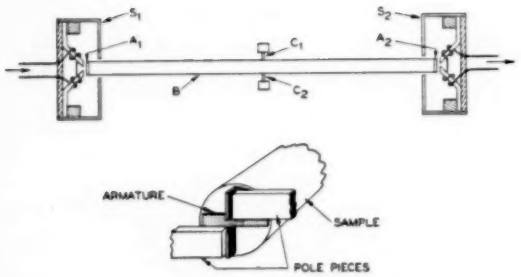

FIG. 1. Schematic of apparatus.

having its center at the axis of the bar. Two short lengths of 0.005-inch piano wire are used, one having its ends attached to the upper pegs and passing under the bar to support its weight and the other fastened to the lower pegs and passing over the bar to contribute a small equilibrating couple. When desired, the measurement at even numbered modes was facilitated by providing a pair of such supports, placed at nodal points corresponding to the particular mode at which the test is made. In the more highly dissipative bars this wire suspension need not be located accurately at a node. The lengths of bar used as test samples varied from about 10 to 100 cm and the diameters from about 0.30 to 2.5 cm. The usual length was about 30 cm and diameter about 1 cm.

The bar is driven to vibrate by alternating current from a variable frequency vacuum tube oscillator acting through a polarized magnetic unit on a thin (0.014-inch) silicon steel armature A_1 of diameter $\frac{1}{4}$-inch. This armature is cemented to the end of the bar with a minimum amount of sealing wax. The magnetic unit is similar in structure to the ordinary bipolar head telephone receiver. In order to obtain good efficiency at high frequencies the pole pieces are made of laminated "45" permalloy and they are inclined as shown in the figure in order to act effectively on the small armature. The resulting vibration of the bar is measured with a magnetic unit identical with that used for driving, but mounted at the opposite end of the bar. The voltage generated in this second unit, as a result of vibration of the bar, is measured by an amplifier-rectifier-meter combination. The separation between the armature and receiver pole pieces on each end is maintained at a known value—usually 0.015-inch. After calibration, the driving force at one end is given by simply measuring the input current, and the velocity of motion at the other end by measuring the voltage generated. For very short bars and at the higher frequencies of test for long bars, it was found necessary to add iron shields S_1 and S_2 for the receivers in order to reduce the inductive transfer of voltage to a value well below that transferred mechanically through the bar.

Determination of the vibratory force applied by the receiver to one end of the bar, and of the amplitude of motion at the other, was made by calibration of the receivers using two methods well known in the art of study and design of telephone receivers.[1] Calibration consists merely in the measurement of the "force factor" of the receivers. When not overloaded this quantity is the ratio of force exerted on the armature to the driving current and this ratio is identical with that of the electromotive force generated in the coils per unit velocity of motion of the armature. This calibration was used for calculating strain amplitudes.

The references show that at resonance of the bar the reaction to the driving force of the receiver is purely dissipative and the velocity of motion is in phase with the force. This reaction, commonly called "mechanical resistance," or sometimes "resistance" because of its analogy to electrical resistance, is obtained from a measurement of the logarithmic decrement per second of the bar and its mass. For longitudinal vibrations of a homogeneous cylinder the mechanical resistance is the product of the logarithmic decrement per second and the mass of the bar. The amplitude of motion for a given driving current may then be measured with a microscope and, with the additional knowledge of the frequency, the resulting velocity of motion may be found. The product of resistance and velocity gives the force corresponding with the driving current. A second method, also described in the references, involves measuring the electrical impedance added to the receiver due to motion of the armature and is sometimes known as the "motional" impedance method. The force factor is the

[1] All essential theory of these measurements is given in *Electrical Vibration Instruments*, A. E. Kennelly. More detailed general theory of dynamics of such structures is in *Theory of Telephone Receivers etc.*, R. L. Wegel, J. A. I. E. E., Oct. 1921.

geometric mean of motional impedance and mechanical resistance.

With a separation 0.015-inch between pole pieces and armature of the receivers used in most of the measurements, the force factor was 1.7×10^6 dynes per abampere or abvolts per cm/sec. which in practical units is 170 dynes per milliampere or 17 millivolts per cm/sec. at 10,000 cycles. This value varied only slightly over the frequency range used. The strains at nodal points of the bar were maintained in the range, 10^{-8} to 10^{-5} cm/cm. The electrical impedance of the receivers at 10,000 cycles was nominally 1000 ohms.

The extreme range of frequency so far used with this apparatus is about 300 to 100,000 cycles. Data taken in this range have been supplemented by a small amount of data taken with the torsion pendulum in the range from about 0.01 to 1.0 cycle.

The modification used for measuring torsional constants of bars is illustrated in the insert in Fig. 1. The armature is cut and tabs bent up at right angles to the end face of the bar as shown. The receiver pole tips are shaped so as to fit with a small clearance into the right angle so formed of the armature. A current through the receiver then exerts simultaneously a torque and an axial force on the bar. The various modes of motion can then be individually selected merely by applying the proper frequency of drive. Calibration for torsional drive was made by the same method as for longitudinal motion.

The procedure of measurement consists simply in adjusting the frequency for a maximum of response for any one resonance and then measuring the range of this resonance by observing the change in frequency required to reduce the amplitude of motion to some convenient fraction of the maximum. The combination then, of the range and frequency of resonance, the mass, length and diameter of the bar, and a knowledge of the form of the particular mode of vibration is sufficient to calculate a gross elastic and a dissipative constant specific to the material of the bar.

An illustrative measurement and calculation

A $\frac{3}{8}$-inch rod of annealed soda lime glass, 48.3 cm long, of mass 86 grams, was mounted with the armature used for measurement of both longitudinal and torsional modes. The frequencies of resonance were found to be 5585 cycles and its approximate multiples and 3572 cycles and its approximate multiples. The first series corresponded to resonance in longitudinal or axial vibration and the second series to torsional modes. Table I gives results of the measurements at various frequencies.

In this table, n is the nominal harmonic number of the resonance, f the actual frequency measured and $\Delta f/nf$ the fractional departure from exact multiple of the fundamental frequency. The deviations Δf were determined by a beat method. It will be seen that the actual frequencies are always less than integral multiples of the fundamental by amounts varying from 0.3 percent to 1 percent. These particular deviations are larger than ordinarily encountered in test samples and are principally due to lack of cylindrical symmetry of the glass rod. This matter is discussed more fully later on.

The column headed r gives the range of resonance. It is the difference in frequency between two sides of the resonance curve at which the amplitude is 0.707 or $1/\sqrt{2}$ of the maximum.

TABLE I. *Dissipation in glass.*

	Longitudinal								Torsional							
n	f	$\Delta f/nf$	r	r/n	R	μ	$h(10^8)$	Q	f	$\Delta f/nf$	r	r/n	R	η	$h(10^8)$	Q
1	5585	0	4.18	4.18	1160	14700	17.0	1340	3572	0	2.92	2.92	407	10850	7.65	1220
2	11100	−.00462	8.1	4.05	2250	7490	16.4	1370	7068	−.0099	5.76	2.88	800	5440	7.45	1230
3	16630	−.0050	12.7	4.23	3520	5230	17.2	1310	10600	−.010	8.20	2.73	1140	3380	7.09	1290
5	27700	−.00361	19.2	3.84	5320	2840	15.5	1440								
6	33350	−.00302	22.9	3.82	6370	2360	15.6	1460	21250	−.0059	15.5	2.58	2150	1590	6.68	1380
7	38960	−.0031	27.3	3.90	7590	2070	15.9	1430								
9	50000	−.00344	34.9	3.88	9700	1590	15.7	1430	31900	−.0058	23.2	2.58	3225	1060	6.68	1370
10	55400	−.00382	35.7	3.57	12700	1320	14.4	1550	35480	−.0062	25.6	2.56	3550	946	6.64	1390
11	61000	−.00405	39.2	3.56	13900	1200	14.5	1560								
14									49900	−.0053	35.6	2.54	4960	674	6.64	1400
15									53500	−.0052	38.2	2.54	5800	628	6.64	1400
18									63600	−.0057	43.6	2.42	6050	498	6.27	1460

These ranges are independent of driving currents provided 10 milliamperes, corresponding to a force 1700 dynes, is not exceeded. At larger driving currents the resonance curve loses its symmetry. This is with little doubt due to the nonlinear performance of such receivers when overloaded and not due to a property of the glass. Values of driving current far below this overload value were used exclusively. In the working range the velocity or amplitude was found to be proportional to the driving force, as though the dissipative reaction were due to an invariable mechanical resistance. The near constancy of r/n in the table shows that this resonant range is not far from proportional to frequency in this sample but does, however, indicate a slow consistent decrease with frequency.

The column headed R is the mechanical "resistance" or the ratio of the driving force to the resulting velocity at the end of the bar measured at resonance. It is a purely dissipative reaction. The units are dynes/cm/sec. and the precision is ordinarily about 1 to 2 percent. The difference in amplitudes of two ends of the bar is far smaller than this precision. The resistances given in this table may be calculated directly from the calibration of the receivers but the accuracy would then depend on the accuracy and constancy of the calibration. This method was therefore not used for this purpose. For longitudinal motion the resistance as previously described is also given by πMr, M being the mass of the bar. The resistance, being proportional to the resonance range, is therefore also very nearly proportional to frequency in this specimen. For torsion the moment of resistance is given by πIr, I being the moment of inertia of the bar about its axis. For the use later made of this quantity it is more convenient to express the resistance as the ratio of an equivalent force acting tangentially at the periphery of the driving face to the resulting linear velocity at the same place. In this case the resistance to rotation is given by $\pi Mr/2$ and is numerically comparable to resistance for longitudinal motion. These resistances to rotation are similarly seen from the table to be nearly proportional to frequency.

On the assumption that the bar is homogeneous and isotropic it is possible to calculate specific properties of the material. The columns headed μ and η (viscosity), h (hysteretic coefficient) and Q (elastic phase constant) represent the specific dissipative property of the glass in three different ways. The first is the effective viscosity, which for longitudinal motion is the ratio of the longitudinal component of stress to the resulting longitudinal dissipative component of strain velocity, all other combinations of either stress or strain velocity being disregarded as is done in defining Young's modulus. This "longitudinal viscosity"[2] is given by

$$\mu = 2Rl/n^2\pi^2 S, \tag{1}$$

where R is the measured longitudinal resistance, l the length of the bar, n the harmonic number and S the cross-sectional area. Since R is nearly proportional to frequency, or to n, this will evidently be, for this material, approximately inversely proportional to frequency. The unit is the ordinary unit used for viscosity called the "poise" and is numerically comparable with values of fluid viscosity. The torsional viscosity is the ratio of shearing stress to the dissipative component of shearing strain velocity and is associated with the rigidity or shear elastic modulus of the material. The shear viscosity is given by

$$\eta = 4Rl/n^2\pi^2 S. \tag{2}$$

The unit is similarly the "poise." For this material it is also nearly inversely proportional to frequency.

The hysteretic constant "h" is the area in ergs of the stress strain loop for unit of volume, per unit of strain squared. This is given by

$$2\pi^2\mu f \quad \text{or} \quad 2\pi^2\eta f \tag{3}$$

for longitudinal and shear stress, respectively. From the table it will be seen that these are nearly independent of frequency, that is, that the area of the stress-strain loop changes very little with the rate of its cyclic traversal. This material might therefore be considered to give a fair example of "hysteretic" dissipation.

For purposes of dynamical calculations it is sometimes convenient to deal with the quantity $\omega\mu$, or $2\pi f\mu$, which like the hysteretic constant, is of the dimensions of elasticity. This may be thought of as the imaginary component of elasticity so that Young's modulus is considered

complex and may be written $E+i\omega\mu$ or $E+ie$, and the rigidity $N+i\omega\eta$ or $N+in$. The tangent of the phase angle of elasticity is designated Q in the table. $Q=E/e$ for longitudinal strain and $Q=N/n$ for shear. For this glass $E=7.23\times10^{11}$ and $N=2.89\times10^{11}$, and Q is in the neighborhood of 1400, being generally somewhat smaller in torsion than in extension. The elastic phase constants of this material are also nearly independent of frequency.

This mechanical phase constant, Q, is analogous to the ratio of real to imaginary components of dielectric constant of many nonpolar solids, which is also nearly independent of the frequency of the measuring applied field. The tangent of the phase angle, or Q, of the dielectric constant for glass is also in the neighborhood of 1000.

Theory and limitations of this type of test

The measurements of stress-strain properties of a material by these methods are not identical with those obtained from cyclic "static" tests. Any type of measurement of the mechanical properties of a material consists in the determination of the relation between force and displacement on a gross sample and from this the stress-strain properties of the material are inferred with the help of a theory of elasticity.

In the "static" test, either the force is arbitrarily applied and the resulting displacement measured, or the displacement is prescribed and the required force measured. To the extent that the theory of elasticity is valid, then, the stress-strain relations may be obtained by simply modifying the units on the force-displacement diagram and the specific properties of the material are then calculated. The principal reactions are elastic and dissipative.

In the "dynamic" or "resonance" method, the displacement is prescribed as a sinusoidal function of time. When the specimen is made a part of a resonant system, the configuration of which is such that the resonance at which a test is made is well isolated from other free resonant modes of the structure and also that all harmonic multiples of any drive frequency used do not coincide with resonance points of the system, then the strain is prescribed by this resonance selectivity, and not by the material, to be sinusoidal and if the arbitrary applied force be sinusoidal, the force-displacement diagram cannot fail to be an ellipse. This is the case with such bars as those measured in these tests. To illustrate the point—suppose a solid material be tested statically and the loop found to have the shape of a magnetic hysteresis loop at some particular amplitude of strain. Next consider what is to be expected when this material is made up into rod form for test, as above described. The static loop may be considered to be built up by almost any periodic stress—for convenience think of this as sinusoidal in time—plotted along the stress axis and a strain represented by a Fourier series, having a fundamental equal to that of the stress and with coefficients which are principally peculiar to the material. Under resonant vibrating conditions in rod form, where the mass and elastic reactions are so large compared with internal friction, the motion is everywhere forced to be substantially sinusoidal and hence the gross strain is forced to be sinusoidal. As a result, the prescribed simple harmonic strain must develop harmonic stresses within the material at the frequency of the strain and its multiples. The component of the strain frequency only will be able to manifest itself as reaction to driving force on the bar. The force-displacement diagram so measured must be an ellipse even though the stress-strain loop is not.

In general it may be said that a resonance test made at one frequency gives only two parameters of a "hysteresis" loop—the slope of an axis and the area. These are correlated with gross elasticity and gross dissipation. In order to get a more detailed description of the phenomenon, additional independent measurements are necessary.

When parasitic losses are satisfactorily eliminated, there remains the interpretation of results in terms of a specific physically significant dissipation constant of the material. It is well known that a rod of material, particularly of metal, has generally a tendency to be longitudinally fibrous and to be harder on the surface than inside. Such material is of course not isotropic and its physical properties, elasticity and dissipation, cannot be completely described by two constants. It is at least very difficult to determine the degree and nature of departure from isotropy.

TABLE II. *Constants of dissipation of various materials.* The approximate frequency specified is not necessarily the fundamental of the particular specimens measured. Whenever the frequency range covered included 10,000~, the values of h and Q were referred to that frequency. The values for slope given in the last column are accurate to ±0.05.

MATERIAL	MODE OF VIB.	APPROX. FREQUENCY	RANGE OF HYST. CONST. h (10^8)	RANGE OF Q	APPROX. SLOPE OF $h-f$ CURVES
ALUMINUM	L	10,000	0.40–2.6	9,000–52,000	−0.29 to −0.17
(Purity:	L	6,000	.31–1.6	13,600–71,000	—
99.5+%)	L	9,000	.25–.43	51,000–88,000	—
	T	10,000	.20–1.3	6,500–41,000	−.24
ALUMINUM (commercial)	L	8,000	.41–1.8	12,000–54,000	—
BRASS	L	6,000	.70–3.8	9,000–50,000	—
CARBON	L	10,000	2.4	1,000	+.03
"	T	10,000	1.2	700	0
COPPER (electrolytic)	L	9,000	3.9–86.0	500–10,000	—
" "	L	10,000	16.0	2,600	−.02
" "	T	10,000	3.3	4,200	−.08
GLASS (soda-lime)	L	10,000	15.0–20.0	1,140–1,330	−.04
" " "	T	7,000	8.0	1,140	−.06
" (Pyrex)	L	10,000	11.0	1,860	0
" "	T	10,000	4.6	1,810	0
HARD RUBBER	L	10,000	21.0	50	+.17
" "	T	10,000	8.0	45	+.21
LEAD	L	10,000	40.0–190.0	37–200	−.10 to −.02
"	T	10,000	46.0	53	−.02
LEAD—ANTIMONY (1%)	L	10,000	60.0	86	+.15
" "	L	1,400	8.6–29.0	230–760	—
" "	T	10,400	60.0	60	+.17
LEAD—CALCIUM (0.04%)	L	10,000	6.0–40.0	150–1,000	0 to .02
" "	T	10,000	27.0	130	.06
MAGNESIUM	L	10,000	.62	23,000	+.11
NICKEL	L	10,000	5.6–30.0	2,000–11,000	+.13 to +.55
"	T	10,000	2.6–8.5	3,000–10,000	+.12 to +.51
SILVER	L	10,000	3.8	6,700	−.10
"	T	10,000	2.0	4,500	−.14
STEEL (drill rod)	L	10,000	1.6–10.0	6,600–40,000	−.13 to +.31
" " "	L	8,000	23.0	3,000	—
" " "	L	13,000	1.5–15.0	4,400–46,000	—
" " "	T	10,000	.64– 1.8	14,000–40,000	−.11 to +.29
" (Vanadium)	L	17,000	2.7–25.0	2,500–25,000	—
" (S.A.E. 5185)	L	10,000	1.8–13.2	3,800–30,000	—
" (" 3250)	L	13,000	2.1–12.1	5,200–31,000	—
" (" 6150)	L	13,000	1.6–18.3	3,500–42,000	—

In such material, when strained, the distribution and magnitudes of strain components vary from point to point and there is no single Young's modulus, shear modulus, or Poisson's ratio which describes the internal properties. In the technical arts Young's modulus and rigidity are useful and indispensible, but in a study of solids as a problem of physics, caution is used in the interpretation of such properties. This attitude applies particularly to the use of such second order effects as internal dissipation. The assumption of isotropy does not introduce discrepancies in order of magnitude between measured and calculated dissipation constants.

In an isotropic rod Young's modulus, E, and the rigidity, N, are related by $E/N=2(1+\sigma)$. This is on the assumption that the influence of dissipation on stress-strain relationships is negligible compared with that of elasticity. The ratio of elastic to dissipative reaction is given by Q, a series of values of which is given in Table II. If in addition it be provisionally assumed that in longitudinal extension of a sample the strain at any point can be considered to be a combination of a pure shear and a pure dilatation in the proportions assumed in elastic theory and that dissipation is associated only with the former, then the longitudinal and torsional or shear viscosities (or h) are related by $\mu/\eta=4/3\times(1+\sigma)^2$. Using σ derived from elasticity measurements and η from torsion measurements, μ was calculated for thirteen materials. In five cases this agreed within 10 percent with measured

[2] See Int. Crit. Tab **5**, 6 (1929).

values. The maximum was 60 percent too high and the minimum 33 percent too low. The average deviation was about 25 percent. Taking these results at their face value, those calculated values which indicate lower dissipation than that measured suggest that the remainder is due to pure dilatation losses such as commonly arise from variation through the solid of any one of the thermal constants such as conductivity, heat capacity or density. Those values which are larger, however, are not so easily accounted for. These considerations seem to indicate, as a primary factor, departure from isotropy; but the closeness of agreement suggests that further study should yield quantitative information regarding this aspect of the physics of such solids. The quantities η and μ are therefore not strictly "shear" and "longitudinal" "viscosity."

The seat of the dissipative process is primarily in those regions in the material where strains are highest, that is in the intercrystalline substance. The strain configuration of any given focus of dissipation must be substantially constant except in amplitude as the frequency is varied. It would therefore seem safe to conclude that the variation with frequency of any dissipation constant in a given sample is significant of the averaged physical process of dissipation although the magnitude of the effect is not.

Sources of experimental error

The accuracy of measurement of resistance, R, is about one or two percent. In most test samples this resistance is due to internal dissipation, and with a perfectly cylindrical sample of isotropic material, the viscosity or hysteretic constant may be calculated to an accuracy equal to that of the measurement of R. In some cases, however (certain aluminum samples) the measured value of R is to a considerable extent due to dissipation at the clamp, air losses, etc., and in one case (a particular fused quartz bar) the principal loss is external. It is proposed here to sketch briefly the nature and extent of these losses.

Clamps. For the longitudinal modes of motion the axial displacement is a minimum and the radial displacement is a maximum at the "nodes." The ratio of axial displacement at the end of the bar to radial displacement at a node is $l/n\pi\sigma r$, σ being Poisson's ratio. For a representative bar $r=0.5$ cm, $l=25$ cm, $\sigma=\frac{1}{4}$, this ratio for $n=1$ is about 60. The effect of dissipation, internal or external, is to introduce in addition a component of axial motion at the node. The ratio of axial displacement at the end of the bar to the axial displacement at the node may easily be shown to be $4iQ/\pi$, or roughly Q in magnitude. The imaginary unit i indicates that the phase difference is $\pi/2$. For the glass specimen this ratio is about 1500, but for some of the more highly dissipative materials the axial and radial components of motion at a node are of the same order that is, a few percent of that at the end of the bar. The maximum tolerable mechanical impedance of a clamp may be precisely defined, but this is hardly necessary as the above considerations furnish qualitative criteria. By virtue of these motions any clamp is potentially a point of drain for energy and it is manifested as an increased measured resistance.

A series of measurements were made on various clamps under different pressures and in different positions. An aluminum bar suspended by silk floss was found to have a mechanical resistance measured at the end, of $R=18$ "ohms." An aluminum clamp made of 1/64-inch sheet, cut so as to fit the surface of the bar at its center and split so as to allow of exerting pressure on the bar, gave added resistance of from 100 to 450 "ohms" depending on the pressure. A brass clamp of the same dimensions gave added resistance of from about 60 to 800 "ohms." A fiber clamp gave values of 10 to 40. This clamp was used in the earlier measurements. More recent measurements on all bars have been made with the wire suspension previously described. The resistance due to this suspension is not over one or two ohms. Other bars will of course be affected differently by the same clamps but experience indicates that with the wire suspension the loss is generally negligible for the specimens measured.

Slip friction. In moving through the air, the bar tends to drag the air at its surface with it and in vibrating sends into the medium a highly damped viscous shear wave. The dissipational resistance encountered by such a vibrating surface may easily be shown from the diffusion form of equation governing the air motion to be $S(\omega\rho\mu/2)^{\frac{1}{2}}$. The constants ρ and μ apply to air

and S is the area of the surface which for the vibrating bar for either mode of motion is effectively one-half the area of the cylindrical surface. For the glass rod at its fundamental frequency this added load is 4.5, which is to be compared with a total measured value of 1160 mechanical ohms. Calculations on practically all bars tested give values of from 1 to 10 with 3 as a usual figure. For bars of the dimensions of the glass bar and having a mechanical impedance less than 100 this correction is not negligible.

This type of loss may be greatly increased by dust or moisture on the surface of the bar. By dusting a little lycopodium powder on a bar near its end a resistance running into hundreds of ohms may be added. Condensed moisture has the same effect. Such extreme conditions never happen in regular routine but it is a part of good technique to keep all test specimens scrupulously clean and dry.

Armature losses. When the end of a bar vibrates in the magnetic field of the receiver, eddy currents are generated in the metal parts, and the iron in the region of varying flux is carried through a magnetic hysteresis cycle. The force of eddy currents is sufficient in aluminum to drive the bar and make a measurement, inefficiently of course, without the use of an iron armature. With the iron armature attached to a quartz bar resonant at 11,300 cycles the resistance in vacuum (5 mm) was 2.5 ohms. The search was not carried farther, but this together with other circumstantial evidence indicates that these losses are of the order of one ohm or probably much less.

Acoustic losses. The resistance added to the measured value, due to dissipation through the generation of sound waves and related mechanisms, is generally the most serious source of error because of its magnitude and capricious variation with frequency. As the frequency of test is varied through the high frequency range where sound waves in air are of the order of magnitude of the diameter of the bar, the added resistance passes through successive maxima and minima, the values of which in extreme cases may run into hundreds of ohms and cannot be predicted with any practicable theory. These reactions are of course principally effective when the sound field configuration is such as to accumulate high pressure at the end face of the bar where its vibration is most sensitive to perturbation. These effects appear principally because of, or through, the medium of the air gap between the end face of the bar and the receiver pole tips. When measurements are not made in vacuum they probably constitute one of the principal disadvantages of this method as compared with that in which the drive takes place through a piezoelectric crystal.[3]

When the air gap is thin, its diameter not too large, and the frequency of test low, the ordinary theory of "air damping"[4] may be applied. The effect is then approximately that of a load of a constant mechanical resistance and elasticity in parallel. When the frequency approaches that in which the diameter of the bar is of the order of the wavelength of sound in air, there is a tendency to approach resonance of radial motion in the air gap, but the simple process of determining the frequency of this resonance by ordinary means is inaccurate owing to large disturbing effects of viscosity and thermodynamic losses. This theory, for the case of circular symmetry, has been worked out and check tests made with the receivers imbedded in a solid plastic in such a way as to present a flat face to the end of the bar. They showed that the added resistance was so high as to make results with low impedance bars unreliable. The alternative was then adopted of removing from the receiver structures all nonessential parts, cases and supports, and making an experimental determination of the magnitude of the lesser effect so obtained. An air gap of 0.015-inch was adopted as standard. The areas of the pole tips were rectangular, $3/32 \times 3/16$-inch and separated by 1/32-inch.

Fig. 2 shows the results of illustrative measurements of dissipative resistance of bars and also, for comparison, the part of this dissipation which is due to air. Resistance including both internal and external dissipation is plotted as a function of frequency. Each curve represents a measurement on a bar over a range of frequencies. In all cases these are, as nearly as the data can be depended upon, straight lines and therefore represent

[3] See works of S. L. Quimby, Phys. Rev. **25**, 558 (1928); K. Röhrich, Zeits. f. Physik **73**, 813 (1932) and others.

[4] I. B. Crandall, *Theory of Vibrating Systems and Sound*, 1926.

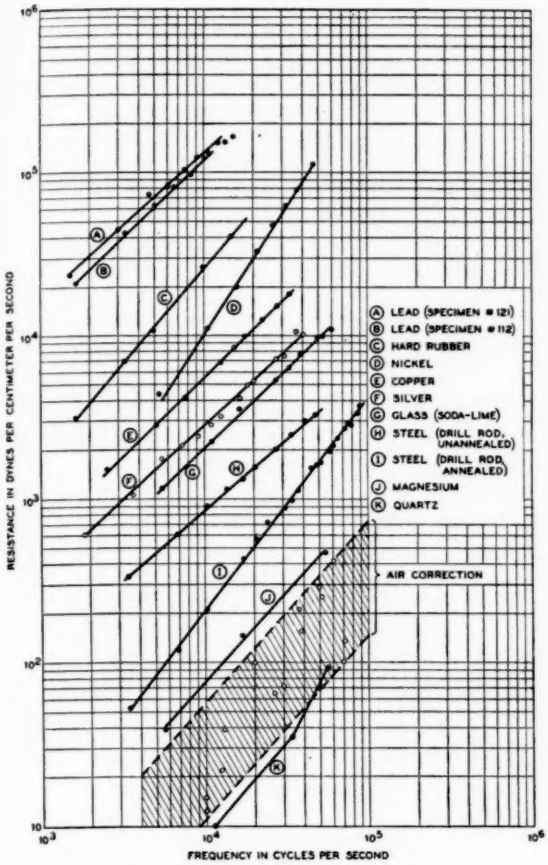

FIG. 2. Mechanical resistance to longitudinal vibration of cylindrical bars measured at some of their natural frequencies.

simple power laws. As an example, a nickel bar shows a resistance at 10,000 cycles of 10,000 mechanical ohms and a slope of 1.54. Other bars show other values. Those given on this sheet are as follows:

Lead	$R = 130{,}000\ (f\times10^{-4})^{0.90}$
Lead	$R = 117{,}000\ (f\times10^{-4})^{0.94}$
Hard rubber	$R = 25{,}500\ (f\times10^{-4})^{1.17}$
Nickel	$R = 10{,}000\ (f\times10^{-4})^{1.54}$
Copper	$R = 5500\ (f\times10^{-4})^{0.97}$
Silver	$R = 2800\ (f\times10^{-4})^{0.90}$
S.L.Glass	$R = 2450\ (f\times10^{-4})^{0.96}$
Drill rod	$R = 840\ (f\times10^{-4})^{0.87}$
Drill rod annealed	$R = 215\ (f\times10^{-4})^{1.31}$

The coefficient is the resistance at 10,000 cycles. It is determined by the size of the bar as well as by the dissipation of material. The two drill rod curves represent the same bar before and after annealing.

The impedances of a number of short bars of relatively low internal dissipation were measured as a function of air pressure at a series of their resonances with the apparatus in a bell jar. At any one frequency the dissipative effect of the air was found to be nearly proportional to pressure, indicating dimensionally a predominance of sound radiation reaction. The differences in impedances measured at atmospheric pressure and at about 5–10 mm of mercury, which represents practically all of the air load, are plotted as circles in the cross-hatched region of Fig. 2. These were all bars of $\frac{3}{8}$-inch diameter. It will be seen that the points are more or less scattered because of resonance effects. At 10,000 cycles the value of the dissipative air load is a matter of 10 to 20 ohms, while at 50,000 cycles it is around 100 to 300 ohms. A single fused quartz bar $\frac{1}{4}$-inch in diameter by about 8 inches long was also measured in air and in a vacuum. The measured points in air for this bar are also plotted. The values in vacuum in this case turned out to be a matter of 10 percent of these plotted points. By examining this picture the degree of dependability of any given curve or point will be evident. The measurement on the small quartz bar shows that its specific dissipation can only be determined by measurement in a vacuum or by otherwise correcting for air losses.

Non-homogeneity and flaws. A lack of homogeneity in test bars is inevitable and varies in amount with the process used in fabrication. The formation of a hard "skin" on cold formed bars is well known. A variation of properties along a bar must also exist to a certain extent. All calculation of specific material properties are of course made on the assumption of homogeneity and the question naturally arises as to what extent, if appreciable, these properties of the sample mask the properties of the material. A hard region near the middle of a bar of steel will introduce a resistance into a measurement at the fundamental mode which is higher than that of a homogeneous soft bar but lower than a hard one. Measured at the second mode this hard spot is not in a region of strain and is not effective. The result is then characteristic of a soft bar. Drill rod is used for making tools in which uniformity is a primary requirement. Samples of this material have always given the most uniform results and

the two curves in Fig. 2 are representative. The measured points fall on smooth curves within the experimental accuracy. In any high impedance bar, properly mounted, the adherence of resistance to a smooth curve may be taken as one index of its axial homogeneity and uniformity. In an effort to check the tests, long bars have been measured and then cut in half, the halves measured, then cut in quarters and measured. The calculations of specific properties gave the same values. A similar test was made by measuring a bar, then cutting equal short lengths from its ends, measuring again and repeating the process several times. The results were always the same as when made at the frequencies of harmonic resonance. These tests indicate that the bars tested are grossly homogeneous.

A bar of drill rod was tested, then cut in two at the middle and cemented together with a film of sealing wax of thickness 0.005 inch. Measurement showed that at frequencies at which a node occurred at the center of the bar the resistance was increased by a factor of five and at other frequencies by about 5 percent. A similar test with a 0.001-inch film showed increased resistance at odd harmonics of 30 to 50 percent and at others imperceptible. By cutting successively short lengths from one end of one of these cemented bars it was found that as the joint receded in effect from a node the effect decreased rapidly and was constant or negligible over a long range in the vicinity of an antinode. This gives a crude qualitative idea of the effect of flaws. They are most likely to show up as irregularities in the measured variation of resistance with frequency.

Variation with frequency of relative distribution of strain components in homogeneous bars of isotropic material

All calculations of specific properties of materials are made on the assumption that the various stress-strain relationships when vibrating at high frequencies are the same as in the static strain. This assumption is not strictly justified, and it is desirable to demonstrate for each test specimen any departure at high frequencies of the strain distribution from its assumed static values. The theory of the ideal cylinder given in Love's *Theory of Elasticity* may serve as a point of departure and leads to the following conclusions.

For torsional vibrations, when a generalized oscillating couple of one frequency is applied at one end of a rod, an infinite number of individual disturbances are sent into the rod. At low enough frequencies, one of these disturbances will be a torsional wave in which particle displacement is in phase along any radius and proportional to its distance from the axis. It is this mode of propagation which is assumed in calculating all torsional constants. When the frequency is below a certain critical value, this is the only true wave which it is possible to propagate, but there is a series of other types of strain sent into the bar which are attenuated exponentially with distance. The sum of these are part of the description of the "end correction." When the drive frequency is increased through the critical frequency, the exponential disturbance of lowest attenuation, that is, the primary contributor to the end effect, suddenly changes in character to a new type of wave superimposed on the first. In this wave the phase change is $3\pi/2$ along the radius and the particle displacement is a Bessel's function of the first order. The next non-wave exponential term which was originally of secondary importance now increases in its effect to take the place of the first transformed disturbance as a potential "end" correction term. As frequency is further increased, a succession of critical frequencies are passed, at each of which the non-wave disturbance of lowest attenuation is transformed from an end correction term into a wave propagation down the rod. Each of these is propagated with very high velocity near its critical frequency but soon approaches that of the original torsional wave as the drive frequency is increased. Since it is desired to work every sample so that the lowest mode is predominant, it is desirable to compare the highest experimental frequency with the lowest calculated critical frequency and to compare the attenuation constant of the lowest calculated non-wave disturbance with the length of the bar. The critical frequencies are $f=xv/2\pi a$, where x is a root of $xJ_0(x)-2J_1(x)=0$, the lowest value of which is 5.136, v is the ordinary torsional velocity and a the radius of the rod. For the drill rod the lowest critical frequency is 660,000 cycles and

all measurements are made well below 100,000 cycles. For the lead alloy samples, this critical frequency is about 200,000 cycles. It is therefore evident that the frequencies of tests for these samples are to be classed as low frequencies. At these frequencies the attenuation constant of the non-wave type of distortion is x/a, and the lowest of these for the two bars mentioned in 13 cm^{-1}, so that any component of force suitable to produce this distortion when applied to the end of the bar is attenuated in the ratio $1/e$ at $1/13$ centimeters or to about 7 percent in 2 millimeters. In a bar having free ends this distortion originates in the reduction of elastic restraint at the end as compared with sections at a distance from it. It must therefore result in a lower resonant frequency, and the bar behaves as though it were somewhat longer in a way analogous with an open organ pipe. This end correction increases slightly in the frequency range used. As a simple test of this correction, measurements were made of departures from multiple values of the fundamental frequency at the frequencies of various harmonics in the drill rod and in the soda lime glass rod. In both cases this departure varied irregularly with harmonic number. In the drill rod the variation in the frequency range 10,000 to 100,000 cycles increased from -0.012 to -0.025 percent and for the glass decreased from -1.0 to -0.3 percent as given in Table I. The drill rod varies in diameter along its length by about 0.02 percent and the glass by about one percent. It appears that the frequency deviation in these specimens is due largely to lack of cylindrical symmetry and that the end correction is negligible. In addition, in view of the uniformity of variation of hysteretic coefficient with frequency, these data represent with accuracy as good as the experiment the dissipation resulting from invariable strain distribution throughout the frequency range.

For longitudinal vibrations the theoretical problem is much more involved but is analogous in some respects with that for torsion. In torsion a simple series of shear waves only are propagated but in longitudinal motion two distinct but bound channels for energy propagation are to be considered. The differential equation of propagation is of fourth order. In torsion there is one type of strain and in elongation two. For longitudinal waves there are two sets of critical frequencies, the bases of each for drill rod being about 500,000 cycles or about five times the highest experimental value. Below this frequency only one wave is propagated and is identical with the well-known "longitudinal" wave of a rod but unlike the low frequency torsional wave, the distribution of strain undergoes gradual variation as frequency is increased. Rigorously considered the "longitudinal" elasticity and dissipation must vary with frequency even though the specific material constants do not. The question resolves itself into a determination of whether or not the relative strain distribution at the highest measured frequency departs from the static distribution by an amount sufficient to invalidate deduction from the data of the variation with frequency of a specific material constant. A calculation of the propagation constant for the drill rod at 100,000 cycles shows an increase of about one percent or a decrease in phase propagation velocity of about one percent. This is very nearly that obtained by means of the usual second order correction for this velocity. Since all singularities in this propagation function of frequency are above 500,000 cycles, relative strain distributions cannot vary by more than about one percent. On this account all calculations of specific constant are to be trusted to about that accuracy. As in torsion, the superposed end strains introduce additional potential energy storage and dissipation which are negligible compared with the experimental error. Experiments have shown, however, that they are much larger than lateral inertia effects. It is taken for granted without the help of rigorous analysis that the assumption of static strain distribution for all frequencies in the rods tested, is justified within experimental accuracy.

Looking further into the details of structure of the solid it would appear that each individual seat or focus of a process of dissipation is subject to an unvarying type of strain or relative configuration of distortion as the frequency is varied. Since, however, because of variation of size and orientation of crystallites in a metal, there is a variation of the elastic constants along any path drawn through the metal, the proper average of which give the shear and Young's modulus, there must be a variation in the ad-

vantage which any focus has in manifesting itself as an integrated part of the gross dissipation measured. Thus a change in gross measured dissipation would result from heat treatment which changed the structure even though the potentiality of every focus for dissipation did not change.

It is concluded therefore that for a sample in a given condition, the variation with frequency of gross dissipation is a direct indicator of certain physical properties of an average dissipative focus, but that its variation with heat or other treatment is in general dependent on other things as well.

Experimental Results

Dissipation as a function of frequency

Fig. 3 shows the calculated hysteretic coefficient for both longitudinal and torsional strains, plotted as functions of frequency for a variety of materials. There are a number of conclusions to be drawn from this figure. The principal point is that the area of the stress-strain loop, of which the hysteretic constant is a measure, under the dynamic conditions of these measurements varies with the frequency of the drive. In some cases (e.g., glass) this area is substantially constant. Usually, however, changes with frequency appear, increasing rapidly in some cases (nickel and annealed drill rod) and decreasing in others (unannealed drill rod). The points in each case fall on straight lines showing that dissipation is a simple power function of frequency. The extremes of the range for materials so far tested are $+0.54$ and -0.31 as the exponent of frequency. Data taken with the torsion pendulum are too fragmentary to report. As far as they go, however, the same type of variation with frequency was observed in the range 10^{-2} to 1 cycle per second. It should be recalled that since the measured resistance of the bar does not change over a wide range of amplitudes the area of the loop under the conditions of this type of test increases in proportion to the square of the strain. Fig. 3 also gives some idea of the relative magnitudes of internal dissipation in the materials tested. It is particularly to be noted that neither the magnitude nor a definite variation with frequency is characteristic of any material. In crystalline materials internal dissipation is primarily dependent on physical structure.

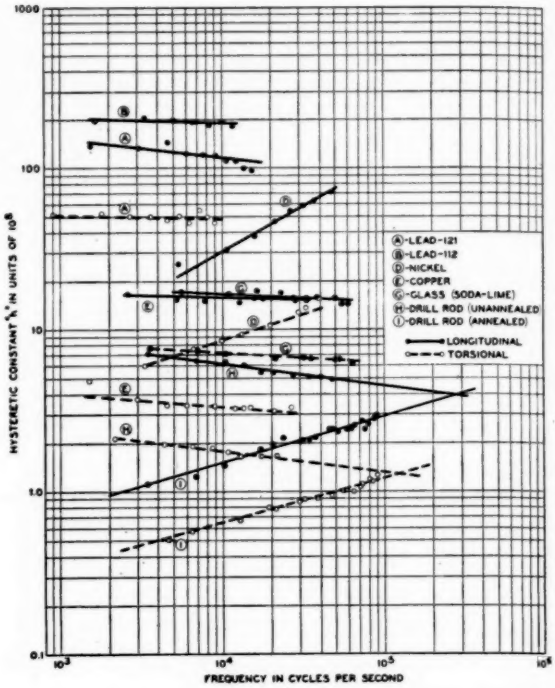

FIG. 3. Hysteretic constant *vs.* frequency for various materials.

A further summary of data for other materials is given in Table II. The column headed "mode" shows whether longitudinal L or torsional T are listed. The reference frequency is 10,000 cycles unless otherwise specified in the third column. The column "range in h" gives the smallest and the largest values of h so far observed. The column of Q gives the largest and smallest observed values of this constant. The column "slope" gives the observed range of the exponent Δ, of frequency to represent h. The accuracy of these figures varies from one measurement to another depending on the number of points taken and on the uniformity of the sample. The maximum uncertainty is estimated to be about 0.05 but in some cases as low as 0.01. Slopes marked 0 cannot necessarily be taken to represent purely "hysteretic" materials.

Internal dissipation and temperature

The change in hysteretic constant between room temperature and 170°C for a few materials is shown in Fig. 4. All substances tested show an

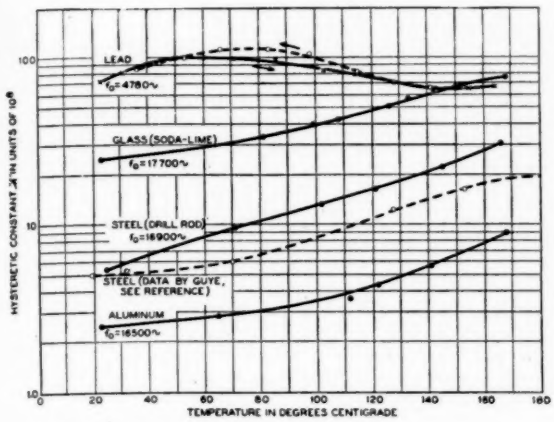

FIG. 4. Hysteretic constant *vs.* temperature.

increase in this range except lead which has a broad maximum at about 80°. Measurements in this case were made both for increasing and decreasing temperature and it will be seen that they are higher on the return path. The time allowed to establish temperature equilibrium in going from one point to the next averaged about twenty minutes. The shape of this loop cannot be due to failure to allow sufficient time to establish temperature equilibrium, as in such a case the curve for increasing temperature should show a maximum at higher values than the curve on the return path. It may not be said that temperature lag is no factor but it is obvious that the lag in change of state or structure of the metal is a large factor. This curve is in accord with ordinary experience that lead may change its state appreciably at these temperatures in the course of an hour or so. Internal dissipation is particularly sensitive to changes of state generally as illustrated by the change due to annealing in drill rod in Fig. 3. It should also be expected that a measurement of the slope of the hysteretic curve with frequency should change with temperature. This is on the presumption that a deviation from constancy with frequency is associated with a mechanism or mechanisms of relaxation, the time constants of which vary with temperature.

Measurements, by means of torsion pendulum, of internal dissipation in a variety of materials have been published by various investigators.[5] The temperature range covered is from that of liquid air to about 1000°C. There is some question as to whether the strain amplitudes should be classed as small, large or intermediate; also as to the time allowed before each measurement for the material to drift toward internal equilibrium at the temperature of test. This point would appear to be important, judging from the curve for lead, Fig. 4, and from aging data of Fig. 9 to be described later.

Internal dissipation, hardness and elasticity in alloy and carbon steels

Fig. 5 shows the effect of heat treatment on certain steels as designated. The material described as vanadium steel is a high carbon steel containing about 0.20 percent vanadium. The steel designated as S.A.E. 5185 is not strictly an S.A.E. standard, but the designation given here is descriptive of it in accordance with the S.A.E. numbering system. For each material a number of samples were hardened by heating to a temperature best suited to the particular material and then quenched to obtain maximum hardness. The internal dissipation, Rockwell hardness, and Young's modulus were then measured on each sample and the average plotted. The temper was then drawn by annealing each sample at a different temperature in such a way as to obtain a variety of hardness values, and the longitudinal dissipation and Young's modulus again measured in each. Each diagram represents the hysteretic constant and Young's modulus measured at constant frequency plotted as a function of Rockwell C hardness. For example, curves I represent vanadium steel measured at 17,000 cycles and it will be seen that as the hardness increases from about 15 up to 60 there is little change in hysteretic constant. This material becomes brittle at about hardness 60 and above this point the hysteretic constant increases by a factor of 7 or 8. Young's modulus changes only by about 5 percent in the complete range of hardness, but its variation is roughly correlated with that of the internal dissipation. This figure also illustrates the sensitivity of internal dissipation to change of state.

[5] Guye and Mintz, Archiv. d. Sci. Phys. et Nat. **4**, 26, 136, 263 (1908); Guye and Freedericksz, Comptes rendus **149**, 1066 (1909); Guye and Schapper, Comptes rendus **150**, 962 (1910); Iokibe and Sakai, Sci. Rep. Tohoku **10**, 1 (1921); Kikuta, Sci. Rep. Tohoku **10**, 139 (1921), and others.

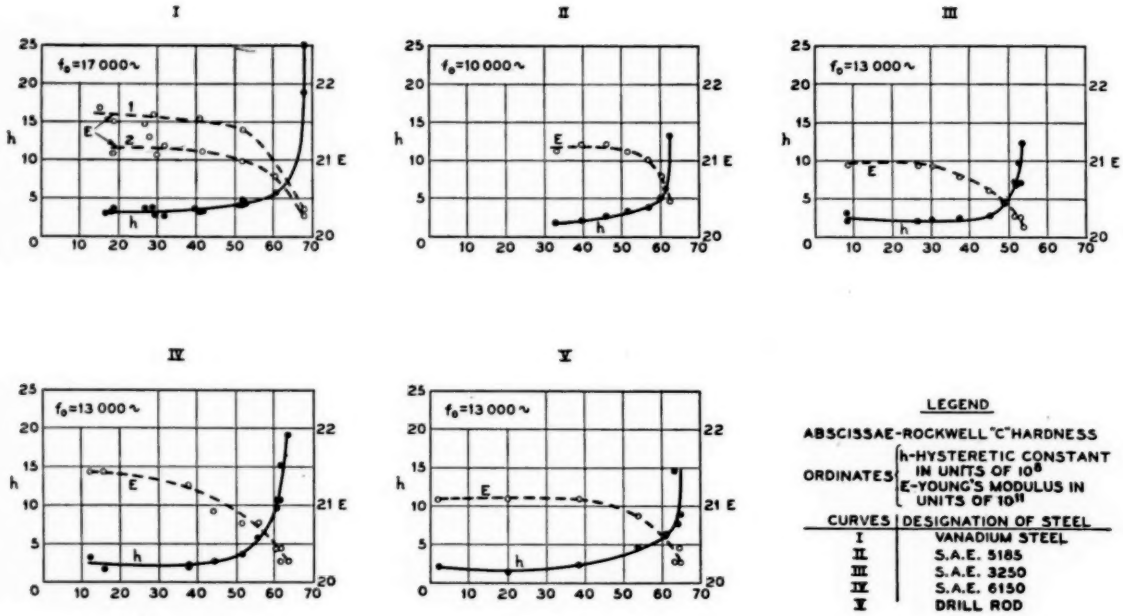

FIG. 5. Hysteretic constant *vs.* hardness, and Young's modulus *vs.* hardness, for various steels.

Effect of annealing hard drawn copper

Fig. 6 shows Rockwell B hardness and the longitudinal hysteretic constant for a series of samples of a variety of hard drawn copper at about 9000 cycles as a function of annealing temperature. A number of $\frac{3}{8}$-inch bars were cut 8 inches long. The hysteretic constant was then measured and the Rockwell hardness measured on the surface and beneath the surface after filing a flat face on the cylindrical surface. Each bar was then annealed for $\frac{1}{2}$ hour in nitrogen at the temperature designated and measurements made. It will be seen that annealing up to a temperature of 250° had very little effect on hardness but that the internal dissipation dropped by a factor of more than 4. Annealing this material at 100° shows an easily appreciable effect on internal dissipation. For temperatures between 250° and 300° very much larger changes take place. In this range, where recrystallization of the material sets in, the Rockwell hardness number drops to less than one-half and the dissipation increases by a factor of more than 16. The results of tests of hardness and particularly of internal dissipation show larger changes in this narrow temperature range than in the rest of the entire range up to 1000°.

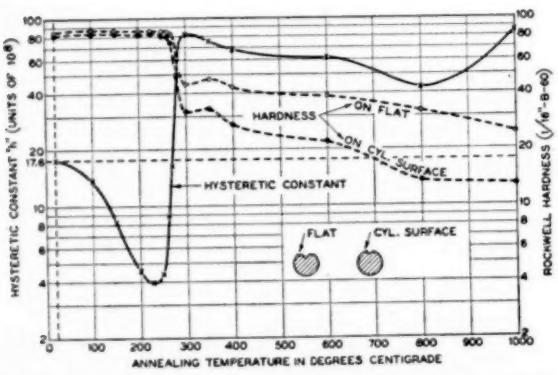

FIG. 6. Hysteretic constant and Rockwell hardness of electrolytic copper rod annealed for 1/2-hour in nitrogen.

Fig. 7 illustrates the variation of hysteretic constant with annealing temperature for commercially deoxidized copper. These samples were in the form of tubes 4 inches long by 5/16-inch outside and about 3/16-inch inside diameter. Measurements in this case were made by suspending the tube with very fine wire and tapping it with a small hammer in such a way as to excite the lowest flexural mode of vibration. The time required for the resulting sound to decay to the threshold of hearing of the observer was then measured by a stopwatch. It was found that by making a small number of such trials, this

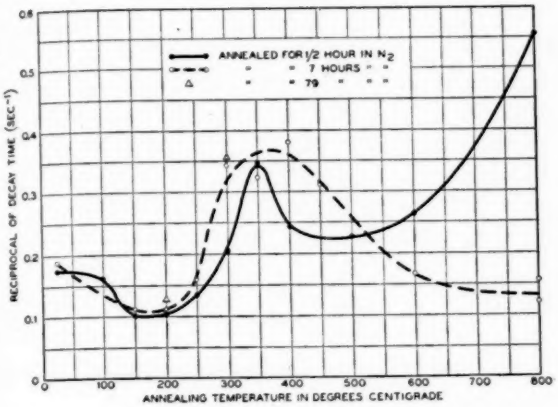

FIG. 7. Ringing test on copper tubes.

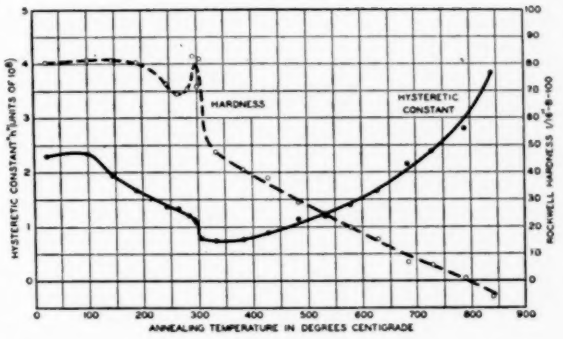

FIG. 8. Hysteretic constant and Rockwell hardness of commercial brass rod annealed for 1/2-hour in nitrogen.

time could easily be measured to an accuracy which showed variations due to heat treatment. The time required, it will easily be seen, is inversely proportional to the hysteretic constant so that the ordinates in this case represent hysteretic constants on an arbitrary scale. A number of such samples in hard drawn condition and very closely uniform as to initial conditions were taken and each annealed in nitrogen at a certain temperature as indicated. In one series, the samples were annealed at specified temperatures for $\frac{1}{2}$-hour and then allowed to cool gradually. In another series the annealing time was seven hours, and two points were measured for annealing time of 79 hours. In the lower temperature ranges, it will be seen that these curves resemble that of Fig. 6 in that internal dissipation drops after annealing at about 200°. A larger change of state occurs in the range 200° to 300°. The increase in dissipation for this range in the case of the $\frac{1}{2}$-hour annealing occurs somewhat later and is less abrupt than in the case for electrolytic copper shown on Fig. 6. This may be associated with a retardation of the recrystallization process due to a small excess of the deoxidizing agent, probably calcium, which is generally present in deoxidized copper. The large increase in dissipation at the highest temperatures, 800° for deoxidized copper and 1000° for electrolytic copper is of interest. This increase of dissipation, however, seems to disappear with longer annealing times. It is impossible, of course, to arrive at any pertinent conclusions without a rather extensive study of the metallurgy of this material.

Effect of annealing brass

A number of pieces of commercial brass rod (approximate composition Cu 62 percent, Zn 35 percent, Pb 3 percent) $\frac{3}{8}$-inch in diameter and 12 inches in length were measured for hysteretic constant and Rockwell hardness for various annealing temperatures and the results are shown in Fig. 8. The changes here are equally as large as in copper but not as abrupt. There is some reduction in hardness and a considerable fall in hysteretic constant up to a temperature of about 300°. The hardness falls more rapidly from then on, but dissipation after a drop of about 25 percent at 300° increases again gradually. The pronounced decrease in dissipation for annealing temperatures up to the beginning of recrystallization of copper and brass and the very marked rise at and above this transition point shows that for a given material mechanical dissipation is an exceedingly sensitive indicator of internal structural change. For annealing temperatures below the recrystallization point internal strains are relieved without accompanying increase in grain size.

In alloys, heat treatment is ordinarily accompanied by phase changes in addition to such structural changes as might be characteristic of a pure metal. The measurement of internal dissipation should be very useful in metallurgical research.

Aging of lead alloys

Fig. 9 shows the change in dissipation during the process of aging in pure lead, lead calcium (0.04 percent Ca) and lead antimony (1 percent Sb) over a period of three years. The three bars

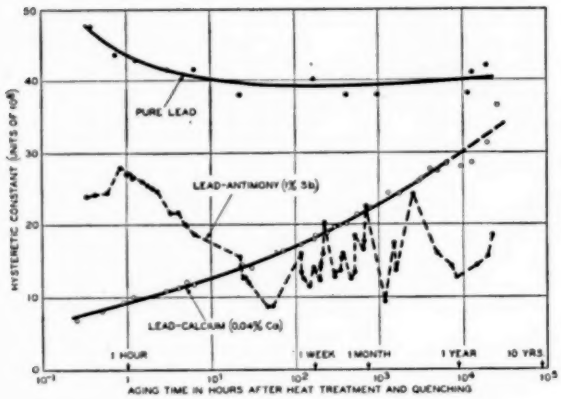

FIG. 9. Aging of lead and lead alloys.

represented were of 5/16-inch diameter and 20 inches long. The longitudinal hysteretic constant was measured only at the fundamental bar frequencies which were 1550, 1450 and 1440 cycles, respectively. At the start the bars were brought into a condition of internal strain by heating to a temperature of 270° and plunging into cold water. The first test was made as soon after this as possible. The samples were kept in glass tubes between tests and subjected to variations of room temperature only.

The pure lead shows a gradual decrease of about 25 percent in internal dissipative power in the course of a day and thereafter varies a small amount irregularly. The initial trend is probably correlated with the relief of very small internal strains which were introduced by quenching and the following small variations to handling.

The lead calcium alloy at the temperature 270° is a solid solution.[6] At room temperature, in the equilibrium condition, this alloy consists of a solid solution of a part of the calcium in lead and precipitated particles of Pb_3Ca, an intermetallic compound. On quenching, the calcium is at first held in statistical dispersion, but after a very short time is chemically compounded with lead. After this the progress of precipitation or diffusion to condensation nuclei of Pb_3Ca takes place slowly. It is presumably the progress toward equilibrium by this last process which is indicated by the curve. The curve drawn has ordinates proportional to the one-eighth power of time.

The lead-antimony was given the same thermal treatment before the test. At the elevated temperatures this alloy is a solid solution of Sb in Pb, and in equilibrium at room temperature the material is a mixture of the eutectic (13 percent Sb) and a solid solution of the remaining part of the Sb in Pb.[7] The curve illustrates the sensitivity of the internal dissipative property in indicating the progress of transition at room temperature from the first-mentioned state toward equilibrium. The variation during the first two days was quite gradual but after this the measurements became very erratic as shown. This specimen was treated with the same care exercised in handling all other specimens. It was found, however, that by simply lifting the specimen from its support and replacing it in the apparatus, the dissipation could be increased by as much as 40 percent. At another time a gentle rocking of the set-up increased the dissipative power of this material by 60 percent. This phenomenon has not yet been studied quantitatively, but it is quite evident that the dissipative power of this material is exceedingly sensitive to small amounts of strain or cold working. The curve shows however, in contrast with lead-calcium, that in a general way the hysteretic constant drops for a day or so and then presumably if not disturbed, tends to settle to a constant value or to a slowly varying condition.

DISCUSSION OF RESULTS

The influence on the vibration of cylindrical bars of that property of a solid through which it dissipates energy when strained has been measured under a variety of conditions. The measurements amount to a direct determination at resonance of the ratio of driving force to displacement of the end of the bar for both longitudinal and torsional modes of motion. The dissipative process is, so to speak, viewed through a sharp resonance which prescribes the strain to be sinusoidal and prevents any component of stress which is not of the same period from manifesting itself directly. The average point strain was maintained within the range 10^{-5} to 10^{-8} cm/cm

[6] E. E. Schumacher. *The Nature of Metals in Relation to their Properties*, Sci. Mo. **34**, 22 (1932).

[7] R. S. Dean, L. Zickrick and F. C. Nix, *The Lead-Antimony System and Hardening of Lead Alloys*, Trans. Am. Inst. Min. and Met. Eng. **73**, 505 (1926).

and the corresponding strain velocities between about 1 and 10^{-5} sec.$^{-1}$. The individual specimens of material illustrate the dissipative property in the class to which they belong but cannot be said to be representative.

For these small cyclic strains the amplitude of motion of the bar at or near resonance is proportional to the driving force which implies that the area of a stress-strain diagram is proportional to the square of the gross strain. If the ultimate mechanism of this process of dissipation is such as in effect to take place in discrete steps then the number of these steps is proportional to strain.

No exception has been found to the rule that over a wide range of frequencies, dissipation is a simple power function of frequency. The effective viscosity of materials varies with frequency to the exponent $(-1+\Delta)$ or the area of the stress-strain diagram at constant strain varies with frequency to the power Δ.

In any single specimen the variation, as expressed by the exponent Δ, with frequency is very nearly the same in torsion and in elongation.

The exponent Δ was found to lie between values of about $-\frac{1}{3}$ (an aluminum specimen) and $+\frac{1}{2}$ (a nickel specimen).

The greatest departure of Δ from zero (nominally hysteresis) was found in polycrystalline metals.

In any one sample the variation with frequency is the only dissipative characteristic which is purely significant of a property of the dissipative focus. Relative magnitudes of dissipation depend on other structural properties.

No change of elasticity with frequency was found. Such changes are expected to be within a fractional amount of the order $1/Q$ and therefore difficult to determine without special technique.

The phenomenon of dissipation in solids must be associated with a process of internal relaxation probably related with or similar to that of "aging" or "creep" but of duration of the order of magnitude of the periods of frequencies of test.

Dissipation in metals is usually greater when the density is greater. This is an exceedingly crude generalization.

In polycrystalline metals, internal dissipation and its variation with frequency is highly structure sensitive. Usually dissipation decreases as the grain size increases, indicating that the principal seat of the process is in the intergrain substance. Any residual small dissipation associated with single crystals has not been measured.

In alloys where phase changes may occur with grain growth as a result of heat treatment, dissipation is not always less for the coarser structure.

Torsional dissipation has never been found to be as large as "longitudinal" dissipation. Calculation of longitudinal dissipation from torsional values, on the assumptions of isotropy and that all dissipation is due to shear, sometimes agrees with measured values but more often does not and may be either high or low, the average deviation being about 25 percent.

Erratum: Electrical Conductivity of Glass. Part I. The Formation of Highly Resistant Layers

Electrical Conductivity of Glass. Part II. Current Increase Phenomena with Highly Resistant Layers

H. R. KIEHL, *Pennsylvania State College*
(Physics **5**, 363, 370, 1934)

IN the two articles entitled, *The Electrical Conductivity of Glass, Part I. The Formation of Highly Resistant Layers* and *The Electrical Conductivity of Glass, Part II. Current Increase Phenomena with Highly Resistant Layers*," in the December, 1934, issue of *Physics*, mention of the Society of Sigma Xi was unfortunately omitted from the paragraph of acknowledgments. The work reported in these papers received financial aid from the Society of Sigma Xi at a time when without such aid continuation of the work would have been extremely difficult. Not only did the timely aid thus received assure continuance of the work at this critical period, but it also began a series of events which made it possible to carry it toward a satisfactory completion. My best thanks are due the Society of Sigma Xi for their timely aid. These papers represent a portion of the work presented in partial fulfillment of the requirements for the degree of Doctor of Philosophy at the Pennsylvania State College.